Quantifying landfill emission potential using a weakly coupled particle filter

Liang Wang[1] and Timo Jaakko Heimovaara[1]

[1]Delft University of Technology

November 8, 2023

Abstract

The emission potential, which represents the total leachable mass in landfill waste body, is hard to measure directly. Therefore we propose to quantify it by assimilating available measurements. The leachate production rate is influenced by the total water storage in the waste body, while both total chloride mass and total water storage in the waste body influence the chloride concentration in the leachate. Thus assimilating leachate volume and chloride concentration simultaneously will help quantify the uncertainties in emission potential. This study investigated the feasibility of using particle filter in a concentration-volume coupled travel time distribution model to estimate the emission potential. Leachate production rates and chloride concentrations were assimilated simultaneously by a weakly coupled data assimilation(WCDA) method. The time lag issue in the travel time distribution model was solved by adding a daily model error to cover layer states. The proposed method was tested in synthetic experiments firstly to investigate the performance. The results show that the uncertainties in chloride mass and waste body total water storage were quantified and reduced. The predictions of chloride concentrations were also improved.

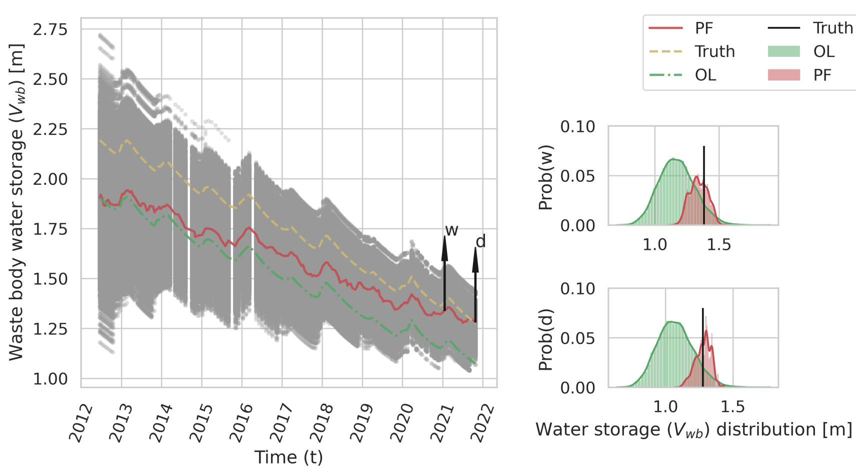

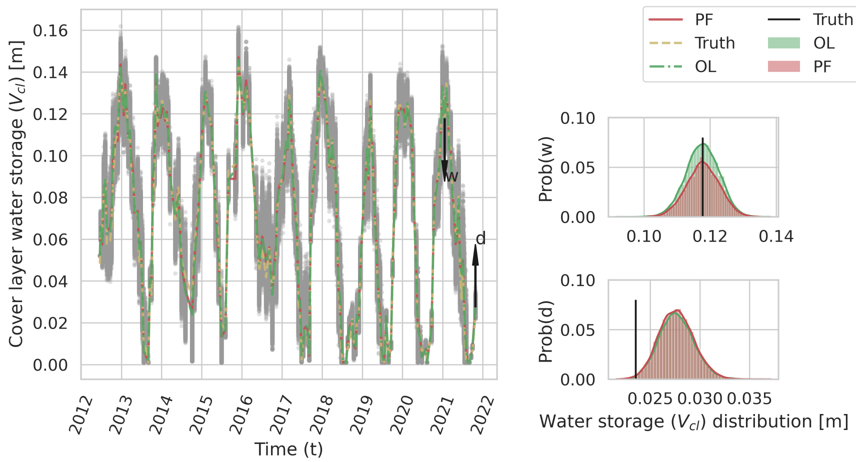
Cover layer water storage (V_{cl}) [m]
Time (t)
w
d
PF
Truth
OL
Truth
OL
PF
Prob(w)
Prob(d)
Water storage (V_{cl}) distribution [m]

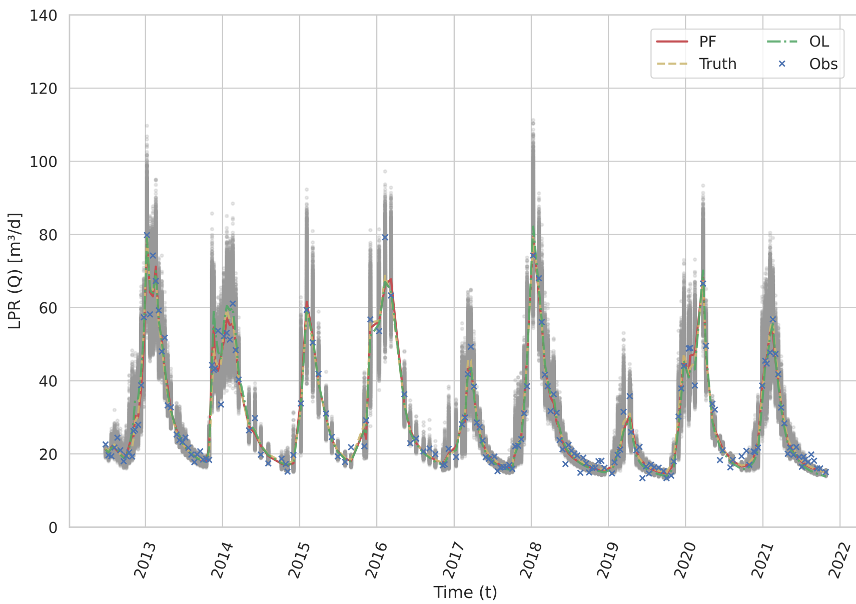
LPR (Q) [m³/d]
Time (t)
PF
Truth
OL
Obs

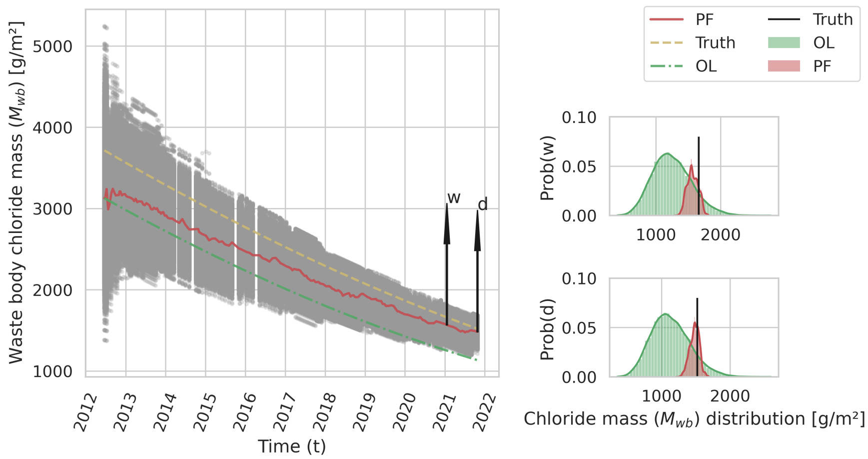

Waste body chloride mass (M_{wb}) [g/m²]
5000
4000
3000
2000
1000
2012
2013
2014
2015
2016
2017
2018
2019
2020
2021
2022
Time (t)
w
d
PF
Truth
OL
Truth
OL
PF
Prob(w)
Prob(d)
0.10
0.05
0.00
1000
2000
Chloride mass (M_{wb}) distribution [g/m²]

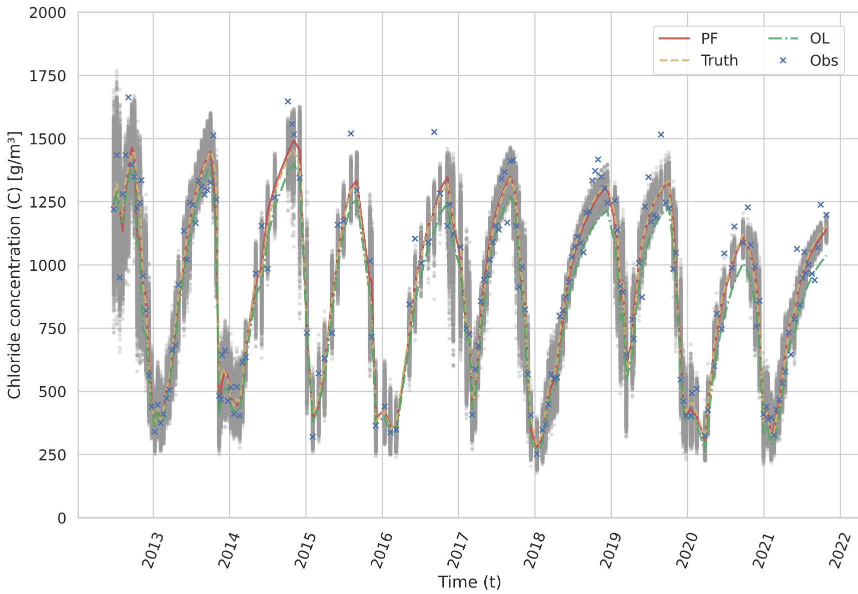

Chloride concentration (C) [g/m³]
2000
1750
1500
1250
1000
750
500
250
0
2013
2014
2015
2016
2017
2018
2019
2020
2021
2022
Time (t)
PF
Truth
OL
Obs

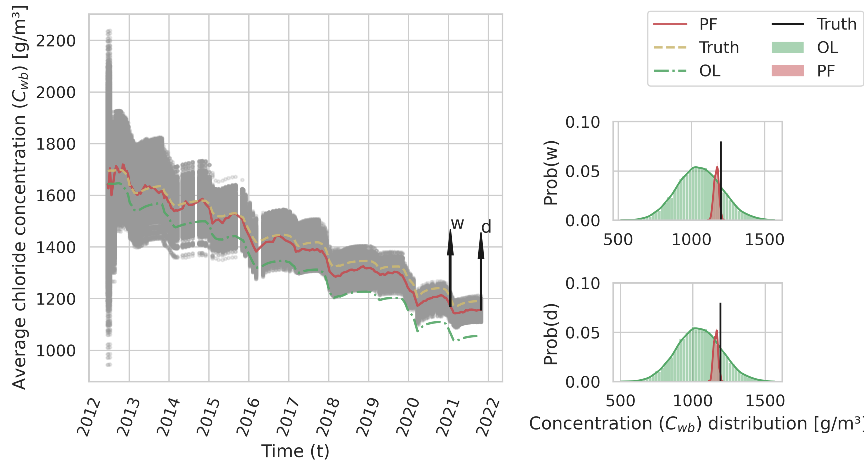
Average chloride concentration (C_{wb}) [g/m³]
Time (t)
w
d
PF
Truth
OL
Truth
OL
PF
Prob(w)
Prob(d)
Concentration (C_{wb}) distribution [g/m³]

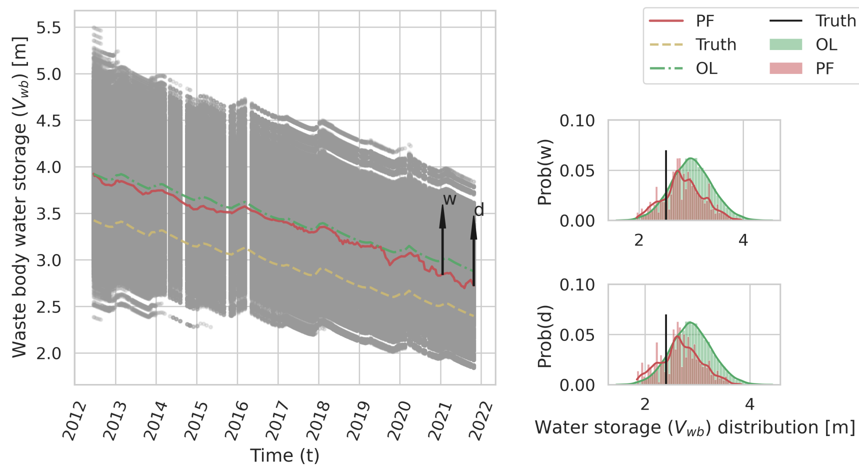
Waste body water storage (V_{wb}) [m]
Time (t)
w
d
PF
Truth
OL
Truth
OL
PF
Prob(w)
Prob(d)
Water storage (V_{wb}) distribution [m]

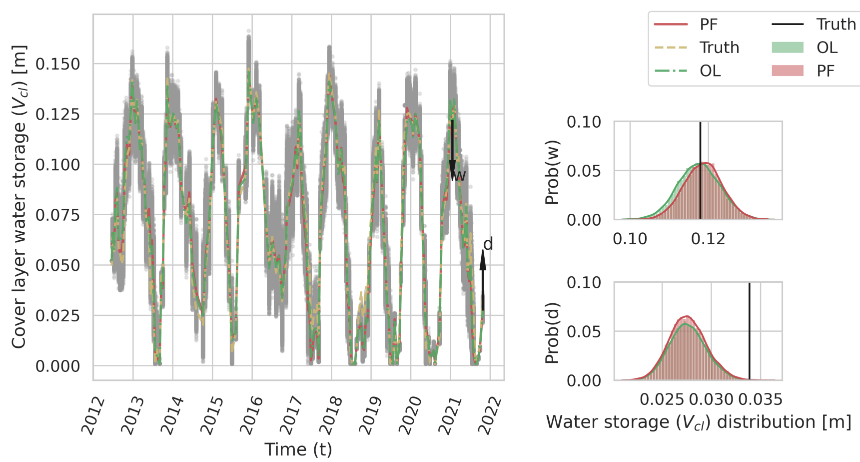
Cover layer water storage (V_{cl}) [m]
Time (t)
w
d
PF
Truth
OL
Truth
OL
PF
Prob(w)
Prob(d)
Water storage (V_{cl}) distribution [m]

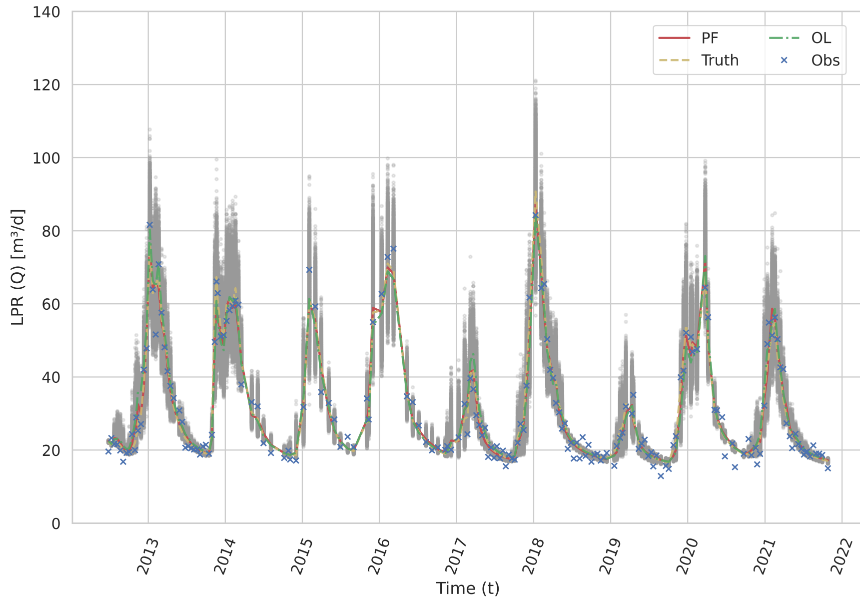
PF
OL
Truth
Obs
LPR (Q) [m³/d]
Time (t)
0
20
40
60
80
100
120
140
2013
2014
2015
2016
2017
2018
2019
2020
2021
2022

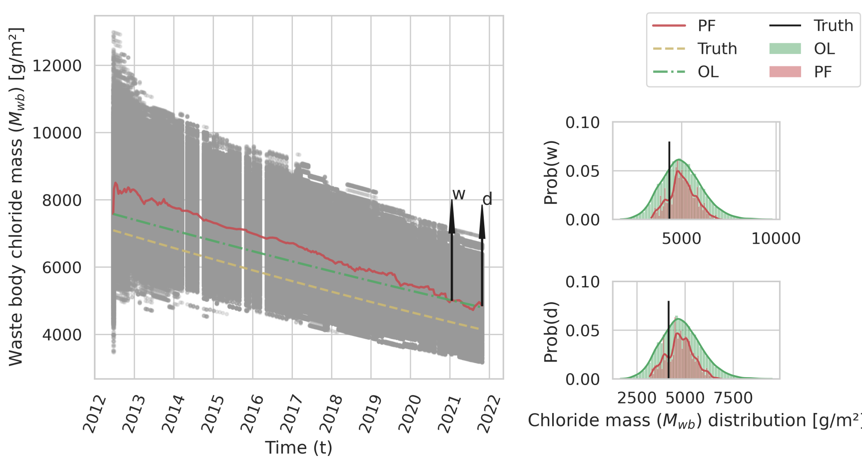
PF
Truth
OL
Truth
OL
PF
Waste body chloride mass (M_{wb}) [g/m²]
4000
6000
8000
10000
12000
w
d
2012
2013
2014
2015
2016
2017
2018
2019
2020
2021
2022
Time (t)
Prob(w)
0.00
0.05
0.10
5000
10000
Prob(d)
0.00
0.05
0.10
2500
5000
7500
Chloride mass (M_{wb}) distribution [g/m²]

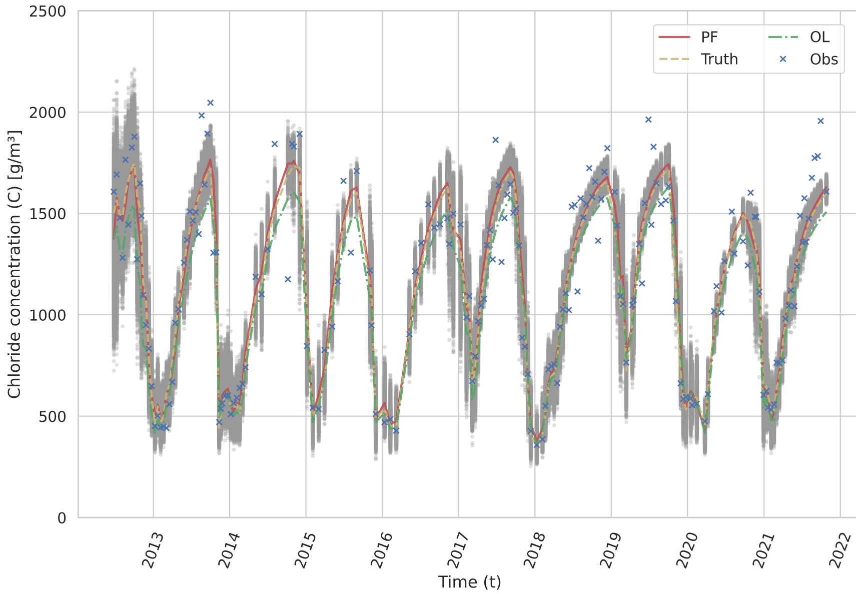
PF
Truth
OL
Obs
Chloride concentration (C) [g/m³]
Time (t)

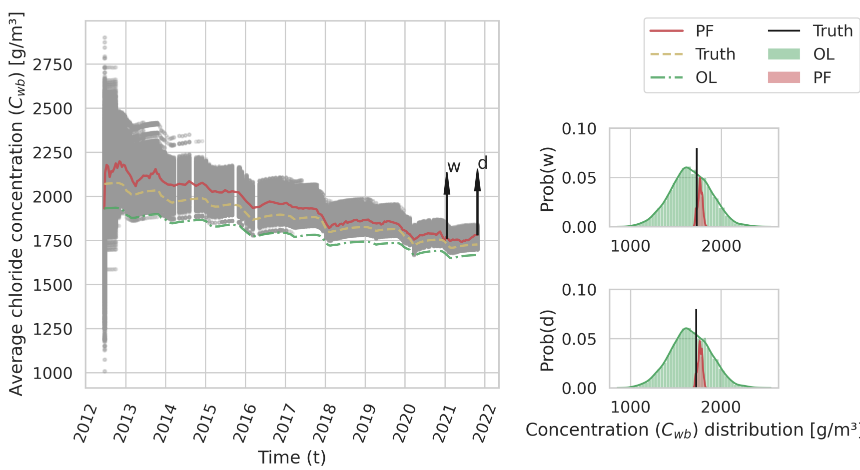
Average chloride concentration (C_{wb}) [g/m³]
Time (t)
w
d
PF
Truth
OL
Prob(w)
Prob(d)
Concentration (C_{wb}) distribution [g/m³]

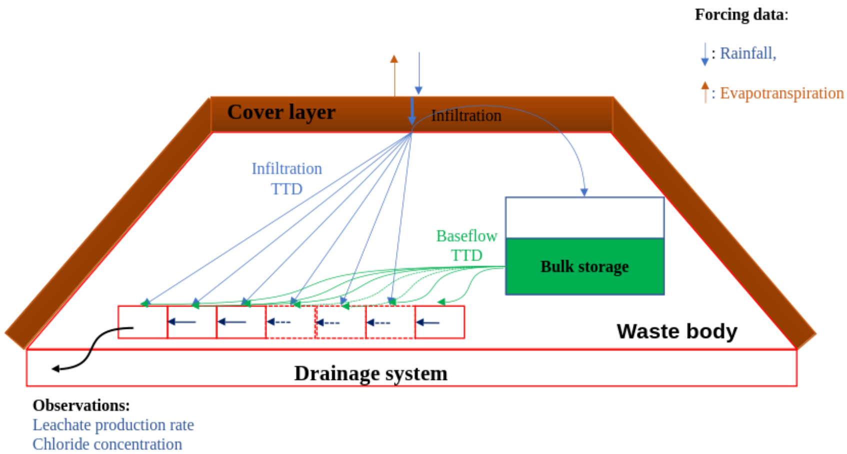
Forcing data:
: Rainfall,
: Evapotranspiration
Cover layer
Infiltration
Infiltration
TTD
Baseflow
TTD
Bulk storage
Waste body
Drainage system
Observations:
Leachate production rate
Chloride concentration

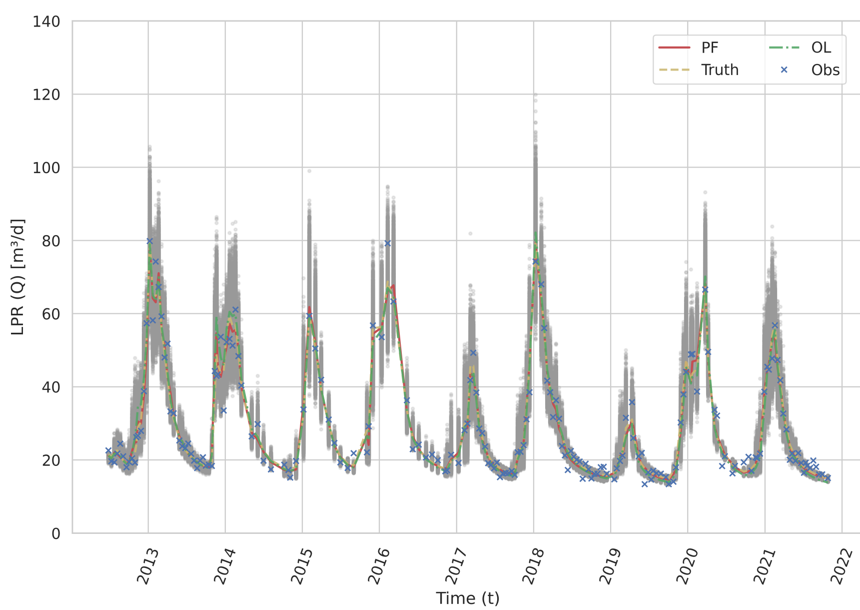
PF
OL
Truth
Obs
LPR (Q) [m³/d]
Time (t)
0
20
40
60
80
100
120
140
2013
2014
2015
2016
2017
2018
2019
2020
2021
2022

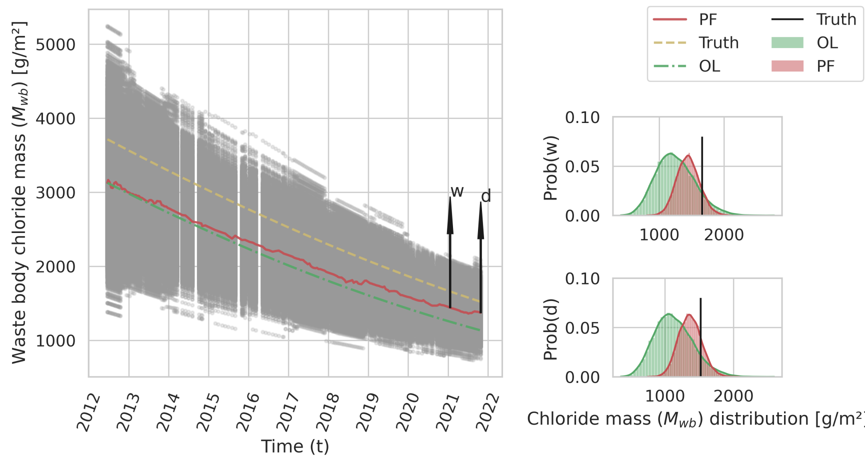
Waste body chloride mass (M_{wb}) [g/m²]
5000
4000
3000
2000
1000
w
d
2012
2013
2014
2015
2016
2017
2018
2019
2020
2021
2022
Time (t)
PF
Truth
OL
Truth
OL
PF
Prob(w)
0.10
0.05
0.00
1000
2000
Prob(d)
0.10
0.05
0.00
1000
2000
Chloride mass (M_{wb}) distribution [g/m²]

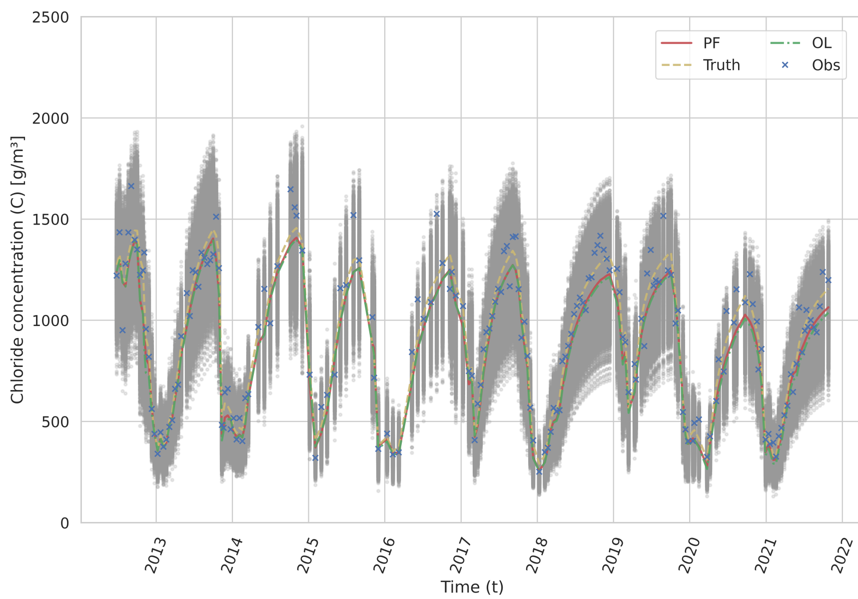
Chloride concentration (C) [g/m³]
2500
2000
1500
1000
500
0
PF
OL
Truth
Obs
2013
2014
2015
2016
2017
2018
2019
2020
2021
2022
Time (t)

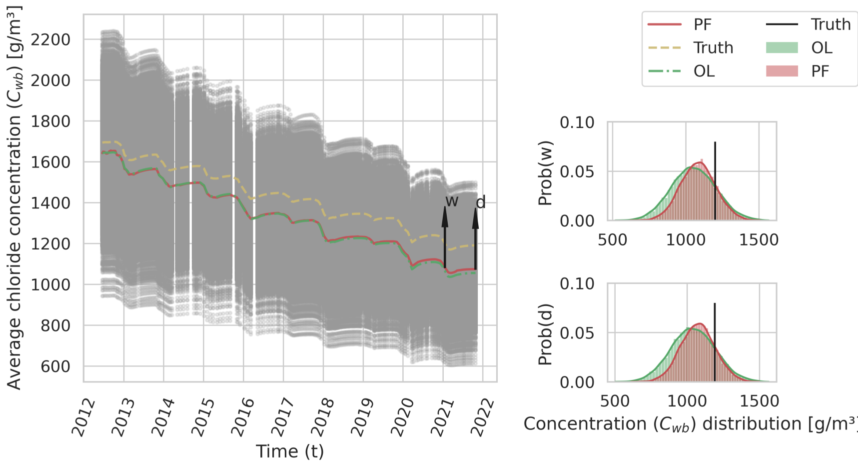
Average chloride concentration (C_{wb}) [g/m³]
Time (t)
w
d
PF
Truth
OL
Truth
OL
PF
Prob(w)
Prob(d)
Concentration (C_{wb}) distribution [g/m³]

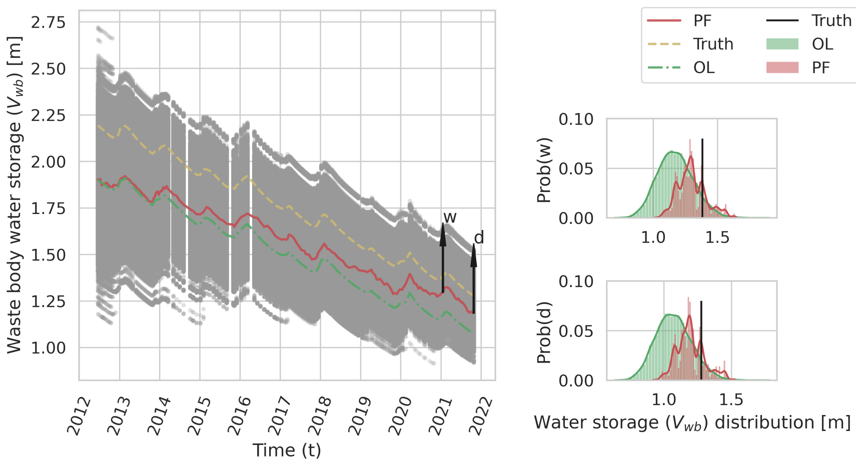
Waste body water storage (V_{wb}) [m]
Time (t)
w
d
PF
Truth
OL
Truth
OL
PF
Prob(w)
Prob(d)
Water storage (V_{wb}) distribution [m]

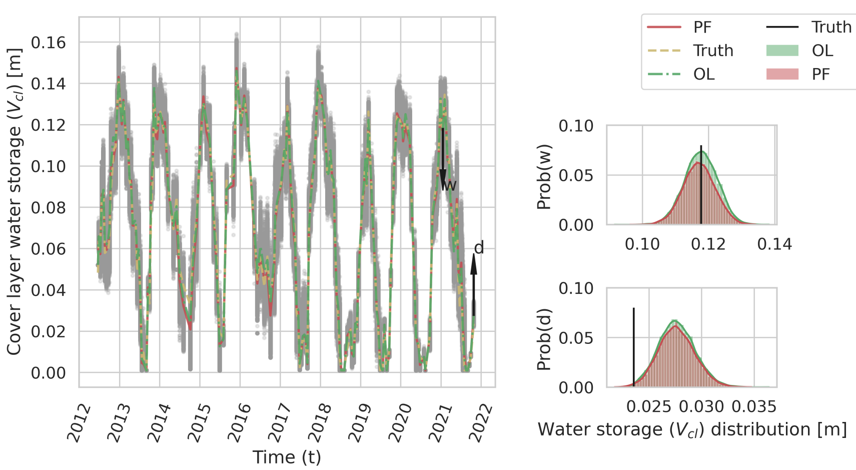
Cover layer water storage (V_{cl}) [m]
Time (t)
w
d
PF
Truth
OL
Truth
OL
PF
Prob(w)
Prob(d)
Water storage (V_{cl}) distribution [m]

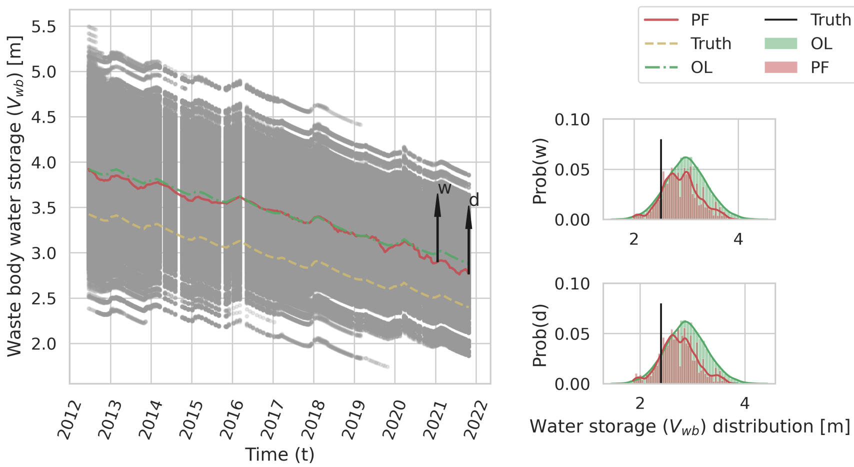

PF
Truth
OL
Truth
OL
PF
Waste body water storage (V_{wb}) [m]
w
d
Time (t)
Prob(w)
Prob(d)
Water storage (V_{wb}) distribution [m]

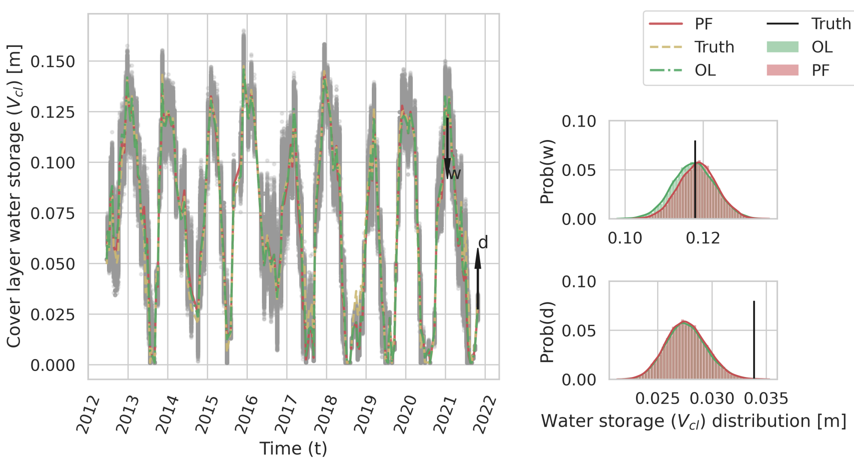

PF
Truth
OL
Truth
OL
PF
Cover layer water storage (V_{cl}) [m]
w
d
Time (t)
Prob(w)
Prob(d)
Water storage (V_{cl}) distribution [m]

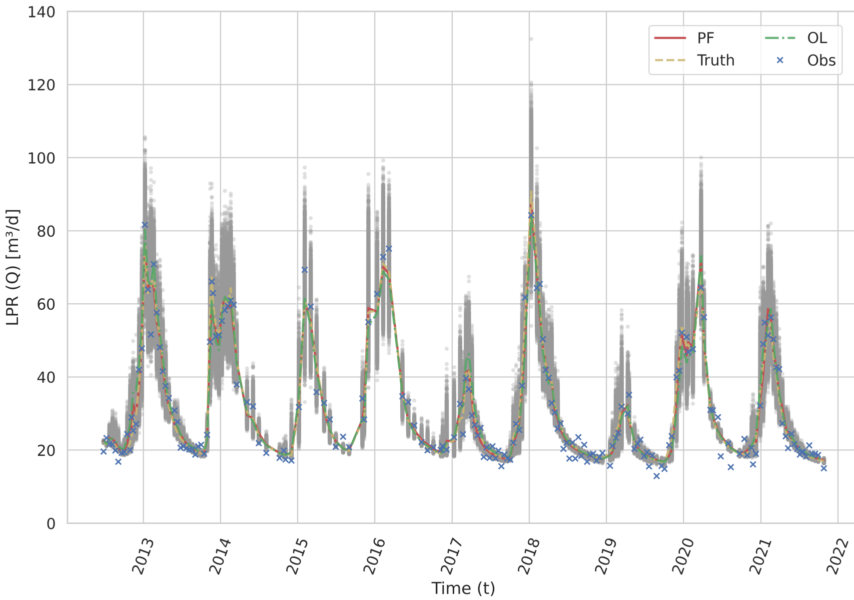
PF
OL
Truth
Obs
LPR (Q) [m³/d]
Time (t)
0
20
40
60
80
100
120
140
2013
2014
2015
2016
2017
2018
2019
2020
2021
2022

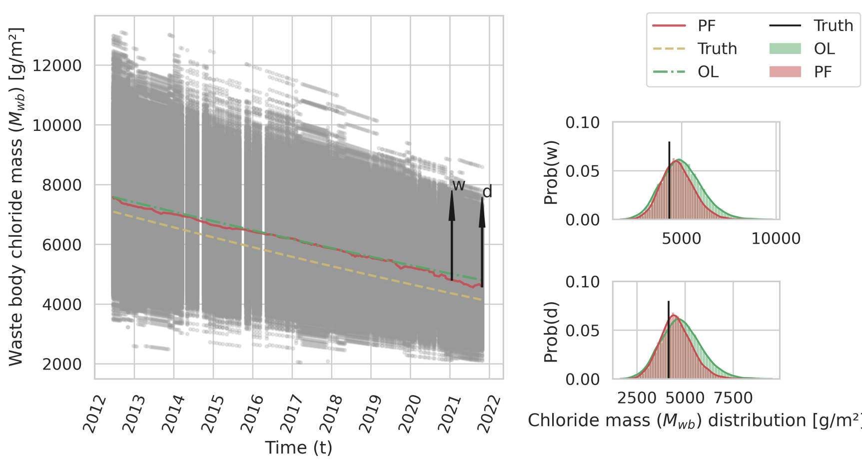
Waste body chloride mass (M_{wb}) [g/m²]
Time (t)
w
d
2000
4000
6000
8000
10000
12000
2012
2013
2014
2015
2016
2017
2018
2019
2020
2021
2022
PF
Truth
OL
Truth
OL
PF
Prob(w)
Prob(d)
0.00
0.05
0.10
5000
10000
2500
5000
7500
Chloride mass (M_{wb}) distribution [g/m²]

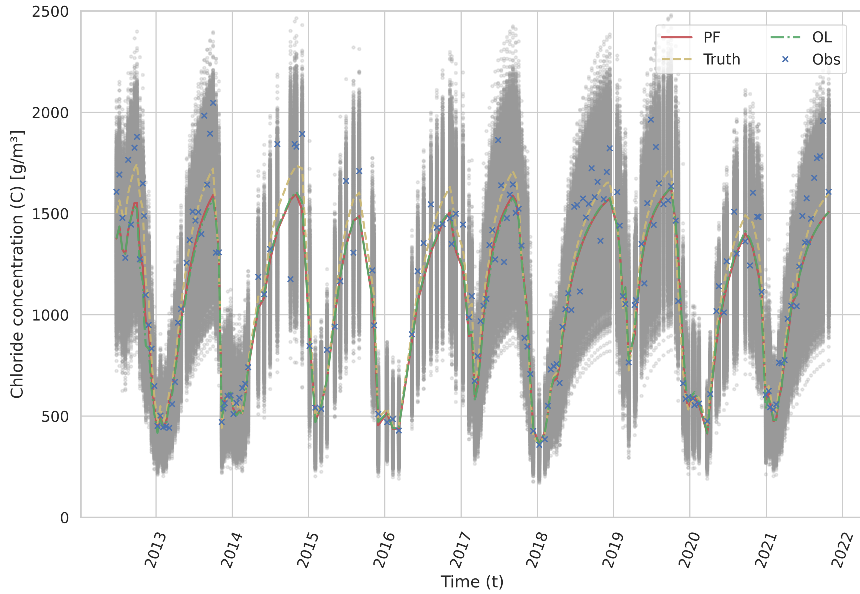
PF
Truth
OL
Obs
Chloride concentration (C) [g/m³]
Time (t)
0
500
1000
1500
2000
2500
2013
2014
2015
2016
2017
2018
2019
2020
2021
2022

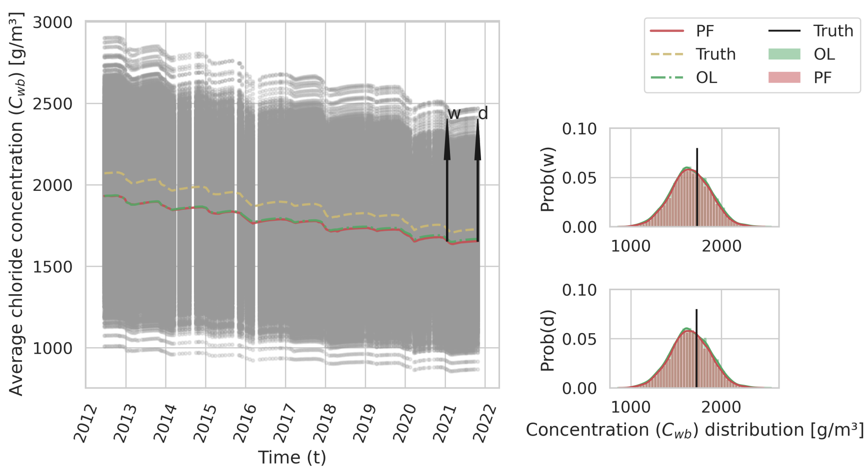
Average chloride concentration (C_{wb}) [g/m³]
Time (t)
w
d
1000
1500
2000
2500
3000
2012
2013
2014
2015
2016
2017
2018
2019
2020
2021
2022
PF
Truth
OL
Truth
OL
PF
Prob(w)
Prob(d)
0.00
0.05
0.10
1000
2000
Concentration (C_{wb}) distribution [g/m³]

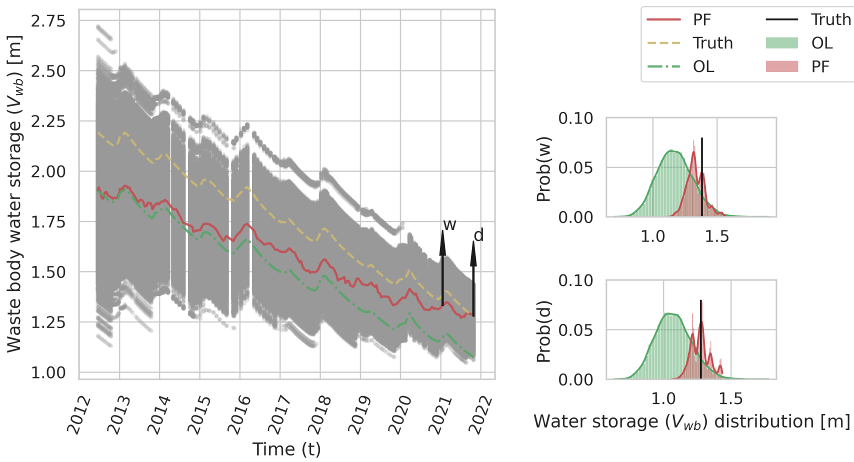
Waste body water storage (V_{wb}) [m]
Time (t)
w
d
PF
Truth
OL
Truth
OL
PF
Prob(w)
Prob(d)
Water storage (V_{wb}) distribution [m]

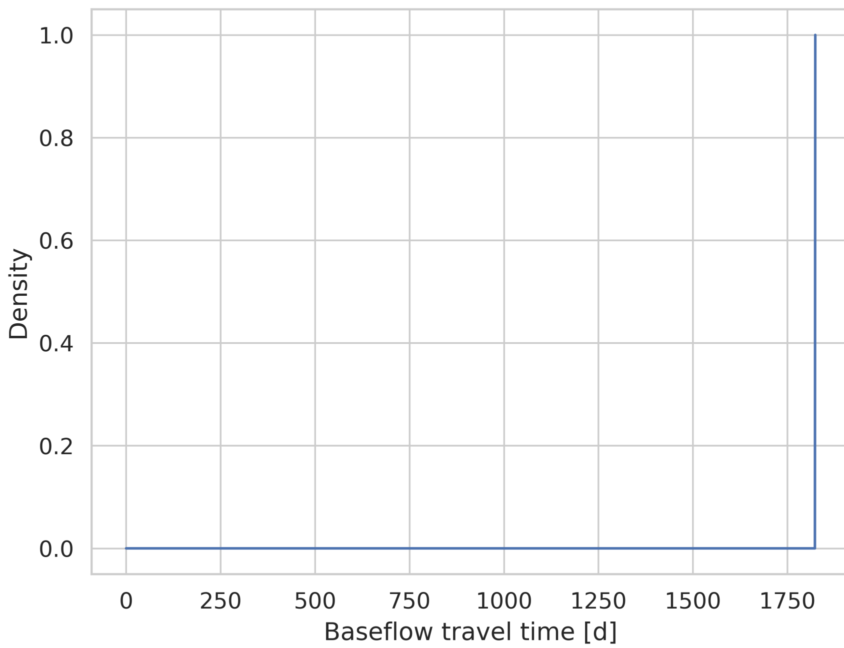
Density
Baseflow travel time [d]

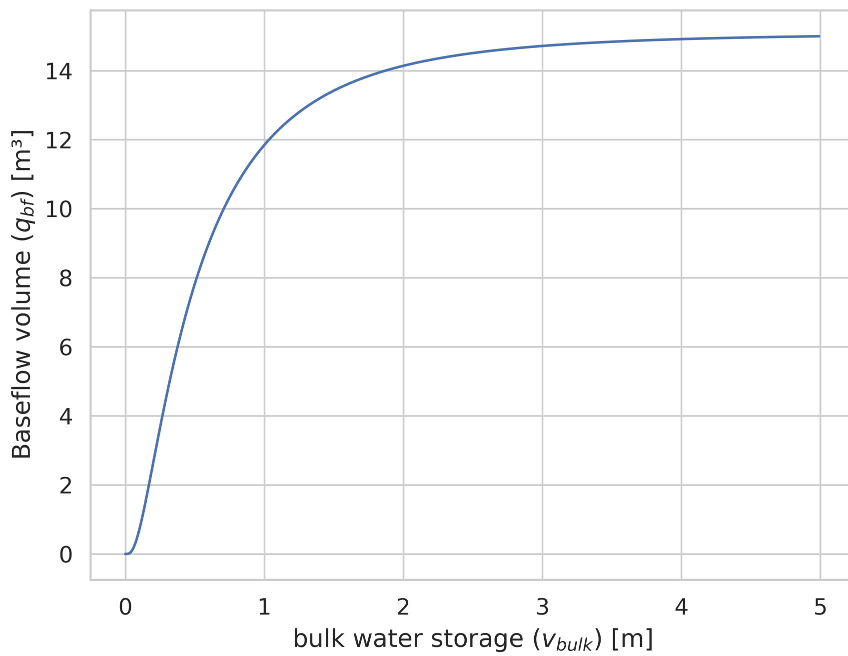
Baseflow volume (q_{bf}) [m³]
bulk water storage (v_{bulk}) [m]
0
2
4
6
8
10
12
14
0
1
2
3
4
5

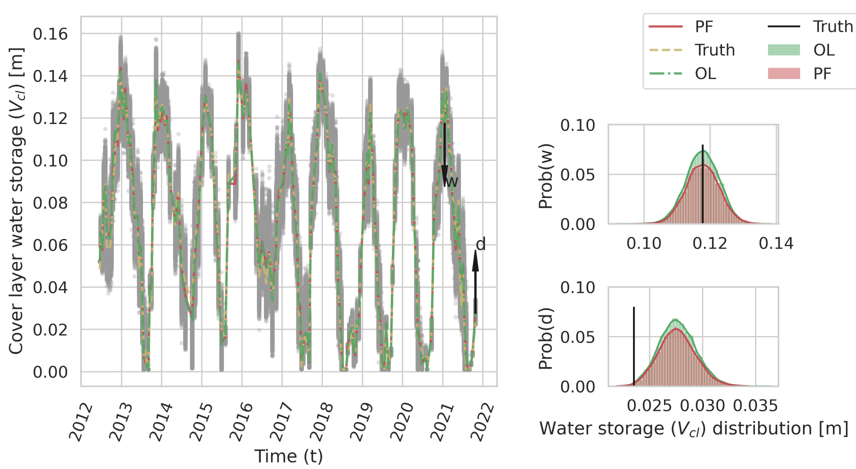
Cover layer water storage (V_{cl}) [m]
Time (t)
2012
2013
2014
2015
2016
2017
2018
2019
2020
2021
2022
w
d
PF
Truth
OL
Truth
OL
PF
Prob(w)
Prob(d)
Water storage (V_{cl}) distribution [m]

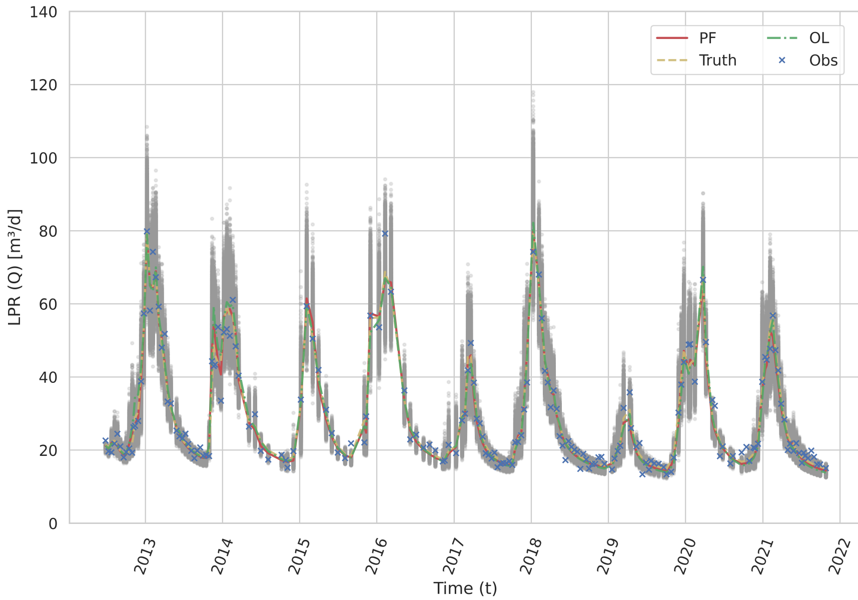
PF
OL
Truth
Obs
LPR (Q) [m³/d]
Time (t)
0
20
40
60
80
100
120
140
2013
2014
2015
2016
2017
2018
2019
2020
2021
2022

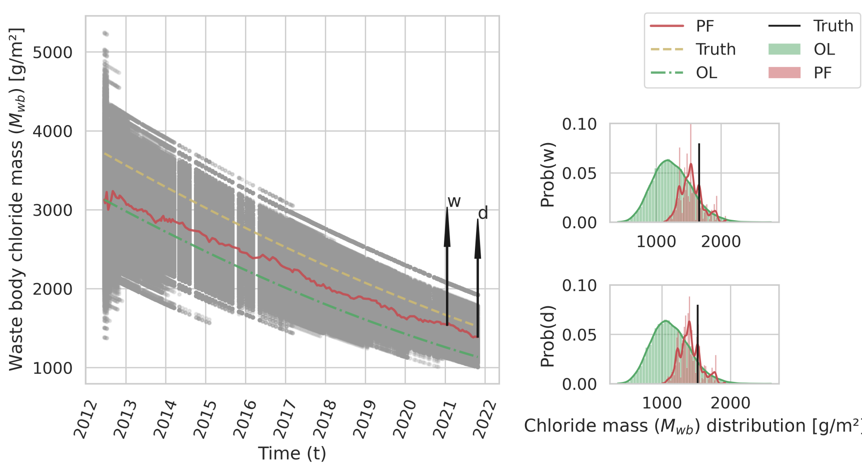
Waste body chloride mass (M_{wb}) [g/m²]
1000
2000
3000
4000
5000
w
d
2012
2013
2014
2015
2016
2017
2018
2019
2020
2021
2022
Time (t)
PF
Truth
OL
Truth
OL
PF
Prob(w)
Prob(d)
0.00
0.05
0.10
1000
2000
Chloride mass (M_{wb}) distribution [g/m²]

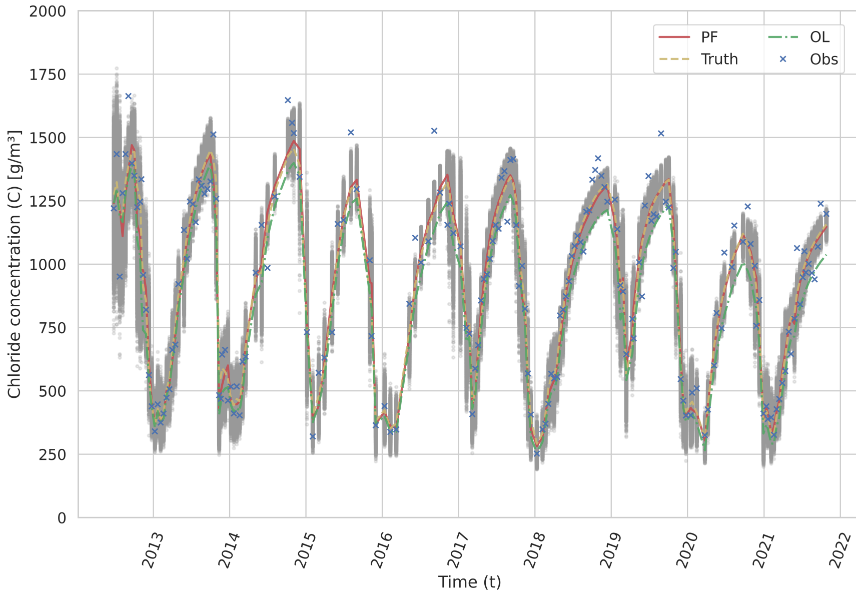
PF
OL
Truth
Obs
Chloride concentration (C) [g/m³]
Time (t)

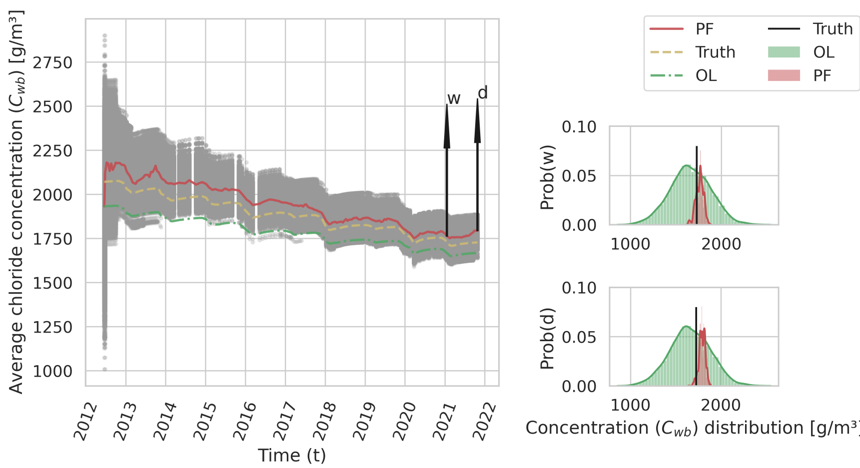
Average chloride concentration (C_{wb}) [g/m³]
Time (t)
w
d
PF
Truth
OL
Truth
OL
PF
Prob(w)
Prob(d)
Concentration (C_{wb}) distribution [g/m³]

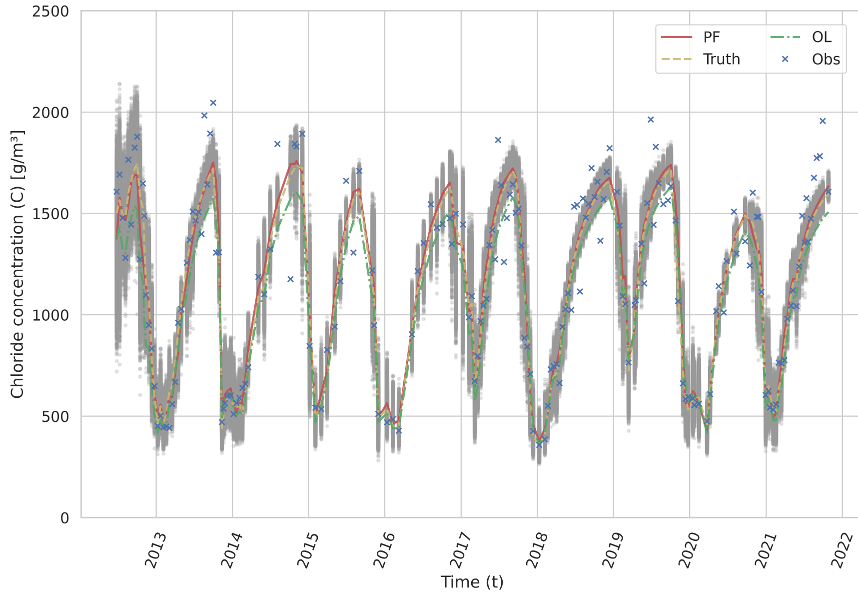
PF
OL
Truth
Obs
Chloride concentration (C) [g/m³]
Time (t)
2500
2000
1500
1000
500
0
2013
2014
2015
2016
2017
2018
2019
2020
2021
2022

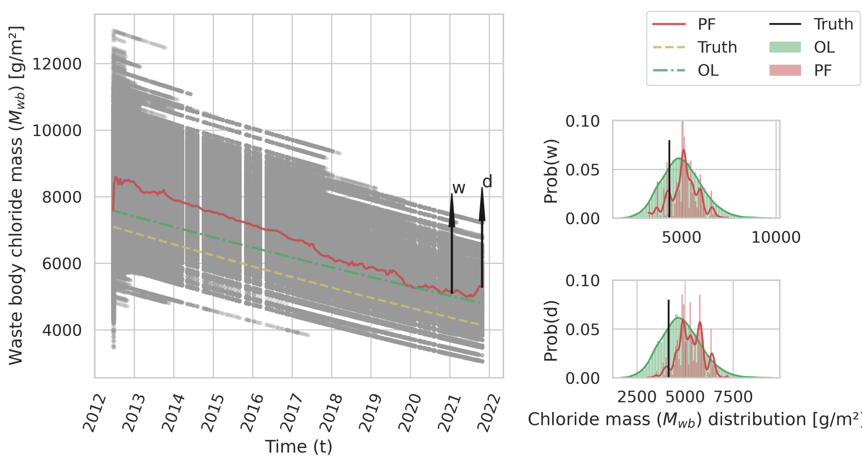
PF
Truth
OL
Truth
OL
PF
Waste body chloride mass (M_{wb}) [g/m²]
Time (t)
w
d
Prob(w)
Prob(d)
Chloride mass (M_{wb}) distribution [g/m²]
12000
10000
8000
6000
4000
2012
2013
2014
2015
2016
2017
2018
2019
2020
2021
2022
0.10
0.05
0.00
5000
10000
2500
5000
7500

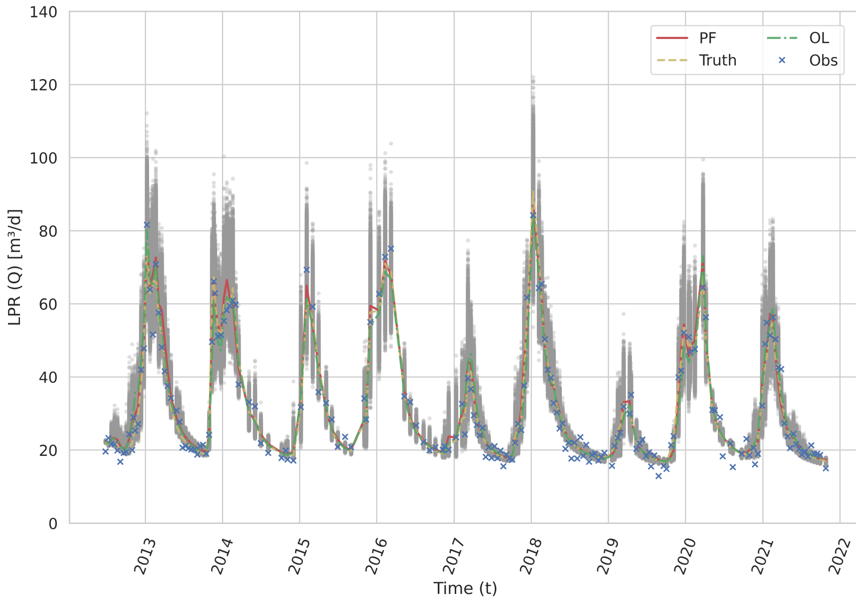
PF
OL
Truth
Obs
LPR (Q) [m³/d]
Time (t)

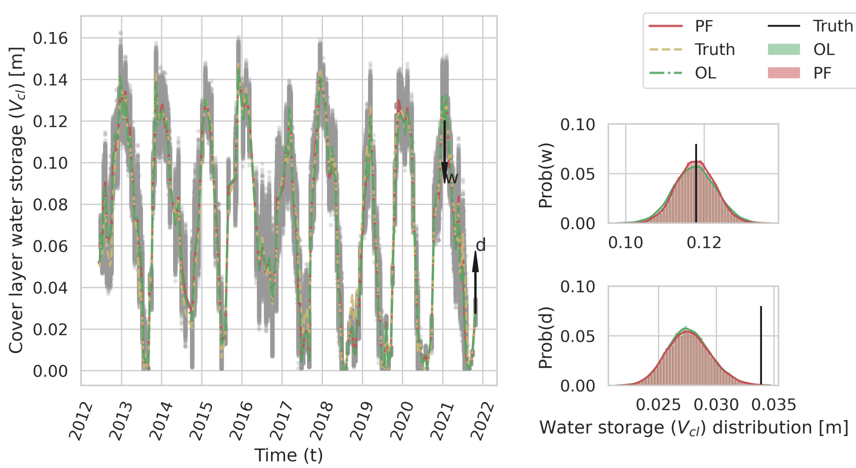
Cover layer water storage (V_{cl}) [m]
Time (t)
w
d
PF
Truth
OL
Truth
OL
PF
Prob(w)
Prob(d)
Water storage (V_{cl}) distribution [m]

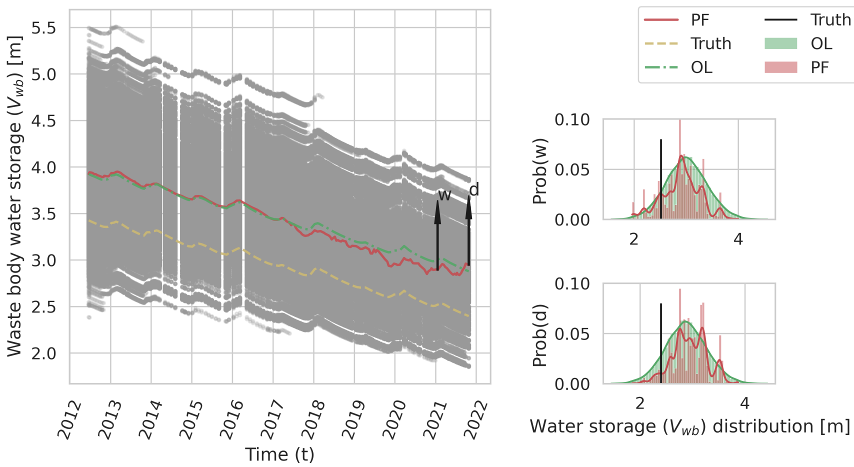

Waste body water storage (V_{wb}) [m]
Time (t)
w
d
PF
Truth
OL
Truth
OL
PF
Prob(w)
Prob(d)
Water storage (V_{wb}) distribution [m]

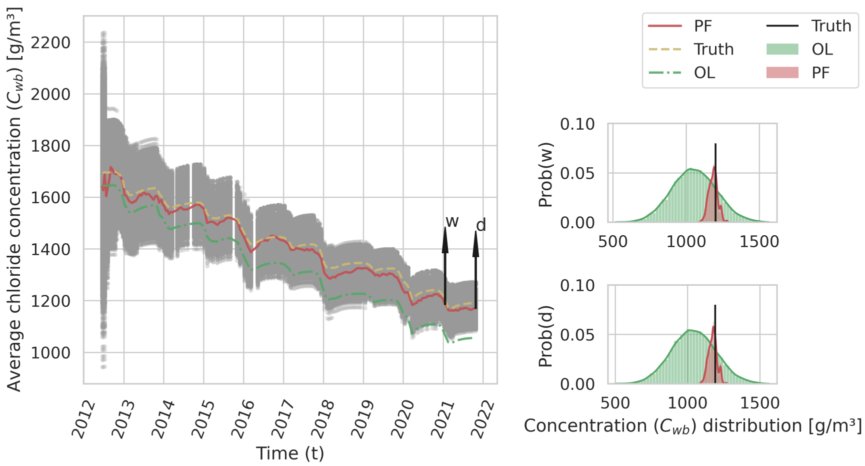

Average chloride concentration (C_{wb}) [g/m³]
Time (t)
w
d
PF
Truth
OL
Truth
OL
PF
Prob(w)
Prob(d)
Concentration (C_{wb}) distribution [g/m³]

Quantifying landfill emission potential using a weakly coupled particle filter

L. Wang[1], T.J. Heimovaara[1]

[1]Department of Geoscience and Engineering, Faculty of Civil Engineering and Geosciences, Delft University of Technology, Stevinweg 1, 2628 CN, Delft, Netherlands

Key Points:

- A new weakly coupled particle filtering method on a travel time distribution model is used for landfill emission potential estimation.
- Analysis clearly demonstrates added value derived from assimilating both leachate production rate and concentration measurements.
- The effectiveness of data assimilation is maximized when the measurable state exhibits a strong sensitivity to the pertinent hidden state.

Corresponding author: Liang Wang, `l.wang-10@tudelft.nl`

Abstract

The emission potential, which represents the total leachable mass in landfill waste body, is hard to measure directly. Therefore we propose to quantify it by assimilating available measurements. The leachate production rate is influenced by the total water storage in the waste body, while both total chloride mass and total water storage in the waste body influence the chloride concentration in the leachate. Thus assimilating leachate volume and chloride concentration simultaneously will help quantify the uncertainties in emission potential. This study investigated the feasibility of using particle filter in a concentration-volume coupled travel time distribution model to estimate the emission potential. Leachate production rates and chloride concentrations were assimilated simultaneously by a weakly coupled data assimilation(WCDA) method. The time lag issue in the travel time distribution model was solved by adding a daily model error to cover layer states. The proposed method was tested in synthetic experiments firstly to investigate the performance. The results show that the uncertainties in chloride mass and waste body total water storage were quantified and reduced. The predictions of chloride concentrations were also improved.

Plain Language Summary

This study presents a method for estimating the amount of harmful chloride in landfill waste and predicting leachate emissions. By combining measurements of water flow (leachate production rate) and chloride concentration, we improved our understanding of total water storage and chloride mass in the waste. Our approach performed best when both measurements were assimilated, and the leachate production rate was sensitive to the variations in water storage within the waste body. The method showed promise in estimating both water storage and chloride mass with correct model parameters, paving the way for future research on understanding uncertainties caused by model parameters.

1 Introduction

Municipal solid waste(MSW) landfill leachate is a primary source of pollution to the surrounding environment because it is a source of contamination for soil and groundwater (Brand, 2014; Gworek et al., 2016; Fatoba et al., 2021). The environmental risk of leachate is determined by its composition and the amount released to the environment. The leachate flux from old landfills is mainly controlled by the water balance of the landfill which depends on precipitation and evapotranspiration. Leachate composition is influenced by the water storage and pollutant mass present in the waste body (Yang et al., 2015; Grugnaletti et al., 2016; Laner et al., 2011). Also, reliable predictions of leachate emissions in the long term require a quantitative assessment of total pollutant mass and water storage in the waste body. As such, this quantitative assessment is an important criterion to determine the aftercare strategy (Kattenberg & Heimovaara, 2011).

Direct measurement of pollutant mass and water storage is virtually impossible due to the size and heterogeneity of waste bodies. Instead, an alternative approach can be used, based on using a forward model predicting leachate flux and composition and simulating the evolution of pollutant mass and water storage in the waste body. A series of deterministic models have been developed to predict leachate production in landfills. Pantini et al. (2014) developed a process-based landfill water balance model where biodegradation and waste compression processes are included. The initial water storage in the model is obtained by a preliminary optimization process. Grugnaletti et al. (2016) got more accurate leachate production predictions by carrying out a step-by-step parameter calibration. It is generally known that the contaminants are leached out from waste through preferential flow (Fellner & Brunner, 2010). J. Zhang et al. (2021) proposed a pollutant concentration, leakage rate, and a solute transport coupled model that allows prediction of concentrations. Quantifying initial values for total water storage in the waste body is required for prediction of leachate production rates, and in addition initial total mass is required when the concentration also needs to be predicted. Generally, the initial values are often approximated by waste characteristics (São Mateus et al., 2012; Yang et al., 2015). However, these estimations could be biased because of the significant spatial variation in initial states and the lack of information on waste composition. Furthermore, some parameters in these deterministic models can be quantified through lab experiments. Nevertheless, similar small-scale laboratory investigations of waste characteristics usually result in wrong estimations of the actual behaviour of full-scale landfills (Fellner et al., 2009).

In recent years, Bayesian inference has been widely applied to hydrology models. It allows for estimating the probability distribution of model parameters by comparing model results with available measurements. We have recently developed a travel time distribution(TTD) model to predict leachate production rate (LPR) and chloride concentration from landfill waste bodies. Parameters in this model are obtained by optimization using the DREAM$_{zs}$ algorithm (Vrugt, 2016), a Markov chain Monte Carlo (MCMC) method for Bayesian inference. The detailed model results analysis will be published soon, and the audience can refer to the supporting information for model equations. Although good pridiction results are obtained in the model, obtaining parameters by fitting or 'history-matching' to data is generally a batch processing method that defines the best fit in an average way. This implies that we get the best fit of the measured data over the whole time range rather than the best estimation of model states. Hence, it cannot recursively benefit from new information from new measurement data to infer model states (Liu & Gupta, 2007). Also, it usually ignores the uncertainty in model structure and input data. Thus, the total water storage and pollutant mass simulation in the waste body could be biased. Significant uncertainty in model states remains, leading to considerable uncertainty in the long-term future prediction of landfill emissions.

Data assimilation (DA) is another Bayesian inference method. It is widely used because of its power to recursively assimilate new measurements to improve understanding of immeasurable or hidden states (Liu et al., 2012; Carrassi et al., 2018). Most DA experiments consist of a forecast step and an analysis step. Model states are propagated with time using a forward model to get predictions, and then measurements are used to filter the predictions in analysis steps. Because of its sequential updating characteristic, it is possible to integrate model, input, and measurement errors.

Among the main data assimilation methods such as Kalman filter (Kalman, 1960) and ensemble Kalman filter (Evensen, 2003), particle filter (PF) (Djurić et al., 2003) is designed to deal with fully nonlinear systems. It has been widely used in hydrology (Plaza Guingla et al., 2013; Vrugt et al., 2013; H. Zhang et al., 2017; Abbaszadeh et al., 2019). Many of the models used with PF, like Hymod (Moore, 1985), are too simple to represent the water and mass transport in landfills. Also, most models used so far only estimate water storage states. We developed the coupled TTD model to predict the leachate production rates and chloride concentrations (see supporting information). Since the concentration states are coupled to the water balance model, we can also estimate the total mass.

The application of DA in the proposed TTD model is a coupled data assimilation (CDA) problem, as the coupled model directly updates both pollutant concentration and water volume states. The CDA is popular because of its ability to make each model component receive information from measurements in other domains (S. G. Penny & Hamill, 2017; S. Penny et al., 2019; Laloyaux et al., 2016; Smith et al., 2015; Tardif et al., 2015). Weakly CDA concepts are developed, where the individual model domains are predicted simultaneously by forward models but updated separately by measurements (S. G. Penny & Hamill, 2017). In strongly CDA, states are updated simultaneously by cross-assimilation of measurements in all domains (Ng et al., 2009), but the required interaction physics between components remains challenging (S. Zhang et al., 2020). Most CDA systems in practical applications are weakly CDA (S. Zhang et al., 2020).

In a synthetic experiment, comparative research was performed by El Gharamti et al. (2013), where an ensemble Kalman filter was used in a 2D subsurface flow-transport coupled model. The hydraulic head and contaminant concentration observations in multiple wells are assimilated to estimate the evolution of these two states. However, hydraulic head can barely represent the water storage in landfill due to the high spatial heterogeneity of water distribution. Also, the risk of losing mass balance in the model exists in ensemble Kalman filter as the model states are adjusted by measurements directly. Particle filtering approaches can preserve the mass balance because the measurements are used to weigh particles instead of adjusting particles.

This study investigates the feasibility of using a particle filtering approach in a landfill TTD model for estimating the emission potential. The emission potential is determined by the waste body's pollutant mass states and water storage states. Based on our knowledge, no research has used particle filtering approaches to estimate both volume quantities and solute concentrations in hydrochemical coupled models. We also believe this is the first time data assimilation has been used to estimate landfill emission potential. Moreover, mass state estimation remains a problem in many data assimilation applications in hydrology. Six synthetic assimilation scenarios were tested to verify the proposed method and optimize the assimilation strategy. Several implementation steps of the algorithm were adjusted to make it suitable for the TTD model. The uncertainties of these hidden states were quantified, and improvement in prediction was evaluated. The chloride mass in the landfill was selected as the representative emission potential in this research.

2 Methods

This data assimilation framework uses a coupled TTD model as the forward model. The weakly coupled particle filter was used as a data assimilation algorithm. The first part of this section describes the theory of weakly coupled particle filter. The second part introduces the forward model and its specific characteristics, which must be addressed in the DA application. The last part concerns synthetic experiment design, implementation procedure, and performance estimation matrices.

2.1 Weakly coupled particle filter

2.1.1 Sequential importance sampling

The weakly coupled PF is based on the sequential importance sampling (SIS) PF. Model and measurement equations are required during the state estimation process as given by Arulampalam et al. (2002). We take $\boldsymbol{x}_t$ to represent a state vector that contains all the model states at the current time step t. Firstly, the state vector is propagated from the former time step to the current step with the model equation

$$\boldsymbol{x}_t = M_t(\boldsymbol{x}_{t-1}) + \boldsymbol{\varepsilon}_{model} \tag{1}$$

where $M_t(\cdot)$ denotes the forward model, and $\boldsymbol{\varepsilon}_{model}$ represents the model error vector caused by different sources of uncertainty. The state vector will then be linked to measurements through the measurement equation

$$\boldsymbol{y}_t = H_t(\boldsymbol{x}_t) + \boldsymbol{\varepsilon}_{mea} \tag{2}$$

in which $H_t(\cdot)$ denotes the measurement operator that connects model states to measured states, and $\boldsymbol{\varepsilon}_{mea}$ represents the measurement error vector.

The main task of state estimation is to estimate the probability density function (pdf) of immeasurable states based on measurement series. We use the subscript $1:t$ to represent the time range from the initial step to step t. Hence, $\boldsymbol{y}_{1:t}$ are the available measurements till current step t and $p(\boldsymbol{x} \mid \boldsymbol{y}_{1:t})$ represents the pdf of current state vector $\boldsymbol{x}$ given $\boldsymbol{y}_{1:t}$. Bayes' theorem is used to calculate $p(\boldsymbol{x} \mid \boldsymbol{y}_{1:t})$, the so-called posterior pdf, by combining prior pdf $p(\boldsymbol{x} \mid \boldsymbol{y}_{1:t-1})$ from last time step with likelihood pdf $p\left(\boldsymbol{y}_t \mid \boldsymbol{x}_t\right)$ as

$$p\left(\boldsymbol{x}_t \mid \boldsymbol{y}_{1:t}\right)=\frac{p\left(\boldsymbol{y}_t \mid \boldsymbol{x}_t\right) p\left(\boldsymbol{x}_t \mid \boldsymbol{y}_{1:t-1}\right)}{p\left(\boldsymbol{y}_t \mid \boldsymbol{y}_{1:t-1}\right)} \tag{3}$$

If the posterior pdf $p(\boldsymbol{x}_{t-1} \mid \boldsymbol{y}_{1:t-1})$ at the previous assimilation step is known, the prior pdf $p(\boldsymbol{x}_t \mid \boldsymbol{y}_{1:t-1})$ could be calculated as $p\left(\boldsymbol{y}_t \mid \boldsymbol{x}_t\right)$ as

$$p(\boldsymbol{x}_t \mid \boldsymbol{y}_{1:t-1})=\int p(\boldsymbol{x}_t \mid \boldsymbol{x}_{t-1}) p(\boldsymbol{x}_{t-1} \mid \boldsymbol{y}_{1:t-1}) d\boldsymbol{x}_{t-1} \tag{4}$$

Then we obtain the aim posterior pdf $p(\boldsymbol{x} \mid \boldsymbol{y}_{1:t})$ as

$$p(\boldsymbol{x}_t \mid \boldsymbol{y}_{1:t})=\frac{p\left(\boldsymbol{y}_t \mid \boldsymbol{x}_t\right) \int p(\boldsymbol{x}_t \mid \boldsymbol{x}_{t-1}) p(\boldsymbol{x}_{t-1} \mid \boldsymbol{y}_{1:t-1}) d\boldsymbol{x}_{t-1}}{p\left(\boldsymbol{y}_t \mid \boldsymbol{y}_{1:t-1}\right)} \tag{5}$$

The core idea of sequential importance sampling is to approximate the required pdf through N independent particles with weight w_i respectively. More specifically, sampling from $p(\boldsymbol{x}_{t-1} \mid \boldsymbol{y}_{1:t-1})$ means several particles are obtained from the previous time step. $p(\boldsymbol{x}_t \mid \boldsymbol{x}_{t-1})$ indicates propagating these particles with forward model (equation 1). $p(\boldsymbol{y}_t \mid \boldsymbol{y}_{1:t-1})$ is a normalization factor in making sure the sum of pdf is 1. Therefore the posterior pdf $p\left(\boldsymbol{x}_t \mid \boldsymbol{y}_{1:t}\right)$ can be calculated as

$$p(\boldsymbol{x}_t \mid \boldsymbol{y}_{1:t}) \approx \sum_{i=1}^{N} w_t^i \delta(\boldsymbol{x}_t-\boldsymbol{x}_t^i) \tag{6}$$

In which δ represents the Dirac delta function. N is the number of particles. The w_t^i is calculated recursively as

$$w_t^i=\frac{w_{t-1}^i p(\boldsymbol{y}_t \mid \boldsymbol{x}_t^i)}{\sum_{i=1}^{N}(w_{t-1}^i p(\boldsymbol{y}_t \mid \boldsymbol{x}_t^i))} \tag{7}$$

The conditional probability $p(\boldsymbol{y}_t \mid \boldsymbol{x}_t)$ is often computed as

$$p(\boldsymbol{y}_t \mid \boldsymbol{x}_t)=\exp\left\{-0.5[\boldsymbol{y}_t-H_t(\boldsymbol{x}_t^i)]^T R^{-1}[\boldsymbol{y}_t-H_t(\boldsymbol{x}_t^i)]\right\} \tag{8}$$

where $H_t(\cdot)$ is the measurement operator, R is the error covariance of the measurements (Van Leeuwen, 2009). Common statistics can be easily acquired with the posterior pdf or weighted particles. For instance, the mean of state vector $\boldsymbol{x}$ is calculated as

$$\overline{\boldsymbol{x}}_t=\sum_{i=1}^{N} w_t^i \boldsymbol{x}^i \tag{9}$$

2.1.2 Systematic resampling

Particle degeneracy is one main limitation of sequence importance sampling, which occurs after several assimilation steps when the weights of all but one particle can be neglected. The effective ensemble size is used to evaluate the degeneracy problem. It is computed as

$$N_t^{eff}=\frac{1}{\sum_{i=1}^{N}(w_t^i)^2} \tag{10}$$

When the effective ensemble size is smaller than $N/2$, resampling should be performed. The idea of resampling is duplicating particles with high weights and discarding those with low weights. After that, all weights will be set as $1/N$. The general resampling algorithms include multinomial, stratified, systematic, and residual resampling methods. In this research, systematic resampling is used as it has good resampling quality. A more detailed description of resampling algorithms is given in Hol et al. (2006).

2.1.3 Weakly coupled data assimilation (WCDA)

Coupled data assimilation is used when there is more than one measurement type. Also, a coupled model should be available. In WCDA, a coupled model is used to predict all the model states at the current time step, while the weighting and updating steps are performed within each component domain. Then the updated states are propagated to the next step by the coupled model. Although the measurements in one model domain are used to update the states in the same domain, the coupled model propagates the information to the other domain(S. Zhang et al., 2020). The details about the implementation of WCDA are introduced in section 2.7.

2.2 Coupled travel time distribution model

The coupled travel time distribution (TTD) model predicts leachate production rates and chloride concentrations. For a detailed description of the coupled TTD model, we refer the readers to the supporting information where we present the governing equations and selected model parameters. Here we briefly introduce the model to help understand the approach.

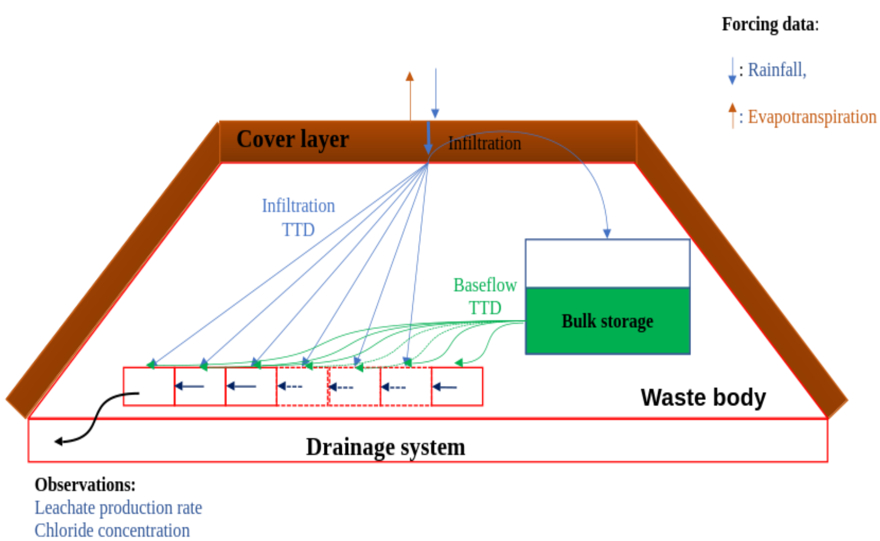

Figure 1. A schematic overview of model structure.

As shown in Figure 1, the model consists of two layers representing a cover layer and waste body in a landfill. The forcing data at the top boundary are rainfall (R) and potential evapotranspiration (Pev), which will enter or leave the landfill from the cover layer. The water storage in the cover layer determines the amount of water (q_{inf}) infiltrating to waste body. The waste body is conceptually divided into a single bulk storage and P cells to represent different travel times of water parcels before they flow out. The time difference between neighbouring cells is one day. So, the leachate in the last cell takes P days to go out. The base flow from the bulk will be distributed to P cells by a baseflow travel time distribution function. Similarly, the q_{inf} from the cover layer is distributed to the waste body with another constant travel time distribution function.

Similar to the transport model from El Gharamti et al. (2013), the chloride concentration is one-way coupled in the water balance model. The concentration states in P

cells are determined by time propagation, as well as distributed leachate from baseflow and infiltration from the cover layer. The parameters and initial states were optimized using DREAM(ZS) (Vrugt, 2016; Shockley, 2020). The state vector is given by

$$\boldsymbol{x_t} = [V_{cl_t}, M_{cl_t}, C_{cl_t}, v_{bulk_t}, m_{bulk_t}, c_{bulk_t}, v_{cell_t^i}, m_{cell_t^i}, c_{cell_t^i}]^T \tag{11}$$

where i represents i th cell state. The concentration defined as $c = m/v$ applies to all elements in the conceptual model. Also, $V_{wb_t} = v_{bulk_t} + \sum_{i=0}^{P-1} v_{cell_t^i}$ and $M_{wb_t} = m_{bulk_t} + \sum_{i=0}^{P-1} m_{cell_t^i}$ are used in the following parts to represent the entire storage states in the waste body. C_{wb} indicates the average concentration in the waste body.We use capital letters to represent the overall state variables of each layer, and we use lowercase letters to represent all internal variables. A detailed explanation of the variables in the model is presented in the nomenclature list.

2.3 Specific model characteristics

2.3.1 One way coupled model

The TTD model we use is based on a one-way coupling between water volume and chloride concentration. The leachate production rates only contain information on water volume states, while the concentration states depend both on water volume and solute mass. However, it is unknown how much information concentration measurements contain about water volume states. Is it possible to only assimilate concentration measurements or do we need both the leachate outflow and concentration measurements? El Gharamti et al. (2013) always use the concentration measurements to update the water head states, while the research does not investigate the benefits of assimilating both measurements compared to assimilating only one. For example, it could be that when assimilating both measurement types, we may get poorer estimation results for volume states when the concentration measurements contain significant measurement errors. In order to explore this issue, we have designed different scenarios to investigate the optimal assimilation strategy.

2.3.2 Time lags in TTD model

In particle filtering approaches, we can estimate hidden states in the model using measurements of observable states because the measurements contain some information about hidden states. Assuming the model is not entirely correct, the model errors will be added to model states during the state propagation process. If the errors are only added to observable states in the state vector, the diversity of hidden states may disappear with resampling. In other words, adding model errors to hidden states gives us the possibility to explore the hidden state space. The hidden states with model error will be assessed in the following time steps because they influence the measurable states. However, if this influence is weak or does not exist, the hidden states will be updated randomly, and the estimation will be poor (Plaza Guingla et al., 2013).

In the forward TTD model we use, we have explicit time lags between many model states and measurements because the travel time distribution considers the time information explicitly. For instance, the oldest cell states will only influence the measurements after $P - 1$ days. This time lag complicates the estimation of multiple hidden states using current measurements. Several studies are trying to solve these challenges with time-lagged measurements in data assimilation (Noh et al., 2013; Li et al., 2013; McMillan et al., 2013; Noh et al., 2014). McMillan et al. (2013) used the current measurements to update states at previous time steps within the time lag. Noh et al. (2013, 2014) used the measurements after an extended time to estimate current model states to consider the time lag effect. These methods use the forward models as measurement operators to link the model states to corresponding lagged measurements. In these approaches, the assumption is that the forward models are accurate for this extended prediction; otherwise, the representation error (Janjić et al., 2018) in the measurement operator should be considered. The maximum time lag in the landfill TTD model we use is around five years. This is much longer than those previously used in distributed catchment models. Consequently, model error accumulation is expected to be severe during the extended prediction process(Noh et al., 2013, 2014), so it is unreasonable to assume a correct model for such a long prediction period. Additionally, the TTD model has thousands of states which are lagged in time, whereas the published applications usually have time lag issues for only one hidden state. To overcome these issues we have developed a specific strategy for the TTD model.

In the TTD landfill model, the cell states are propagated with time. After P (the number of cells) days, there will be a connection among all cells and bulk states. We call this implicit relationship 'history'. We can estimate hidden states by current measurements if this' history' is maintained. Hence, the initialization of particles and the model errors should guarantee this 'history'. The implementation strategy is further explained in section 2.7.

2.4 Site and data description

The model parameter calibration is based on actual measurements from the Braambergen landfill in the Netherlands (Duurzaam stortbeheer, 2023). Daily meteorological forcing data (same as model resolution) are obtained from the nearest weather station affiliated with Royal Dutch Meteorological Institute (KNMI) (2023). The leachate is pumped out from the drainage system, and the daily production volume is acquired. The chloride concentration is measured by sampling from the drainage layer generally with a bi-weekly frequency(with some larger intervals up to 28 days). In practical cases, there are many irregular values in daily production rate measurements because of the management of the leachate pump system by the landfill operator. When the pump system is broken, the outflow remains in the drainage layer, resulting in an observed leachate production volume of zero. Afterward, the water is pumped out, a large leachate volume is measured. In order to limit the effect of these operational irregularities, seven days' average leachate production rates were calculated from the cumulative leachate measurements and used as measurements. The measurement equations for leachate production rate and chloride concentration are:

$$LPR_t = \frac{\sum_{i=t-6}^{t} v_{cell_{0_i}}}{7} + \varepsilon_{LPR_{mea}} \tag{12}$$

$$C_t = c_{cell_{0_t}} + \varepsilon_{C_{mea}} \tag{13}$$

2.5 Synthetic truth generation

Synthetic experiments are often designed to evaluate the performance of data assimilation techniques. Artificial truth states are generated by running a known forward model. If the DA algorithm is effective, estimated states or parameters are expected to converge to the synthetic truth by assimilating the simulated measurements obtained from the forward model. The method of creating artificial truth is highly dependent on the aim of the applied DA technique and the assumption of existing underlying uncertainties. The primary sources of uncertainty for a deterministic model are errors in forcing data, initial states, model parameters, and model concepts. The most simple scenario assumes that the model is correct and only adds white noise to simulated measurements as measurement error. Weerts and El Serafy (2006) perturbed forcing data to consider the forcing data uncertainties in a state estimation problem. Plaza Guingla et al. (2013) further added Gaussian noise to model parameters, although only model states are updated in that research. Li et al. (2013) chose to perturb the state variables in a probability-distributed hydrological model. All the uncertainties above are considered to be included in state variables. Gelsinari et al. (2020) used the 'truth' generated from the unperturbed model, while the model used in assimilation is with a perturbed parameter set. Since we aim to assess the feasibility of estimating emission potential in the TTD model by coupled particle filter, we assume the forward model parameters to be correct in order to simplify the problem. The initial states and input data were perturbed in order to simulate a scenario where we have a poor understanding of initial states, and the input measurements are inaccurate.

The initial states in 2003 were obtained from model calibration in order to generate a synthetic truth. Zero mean Gaussian error with a standard deviation of $10\% \times c_{ini}$ and $10\% \times v_{ini}$ were added to perturb the initial states. Zero-mean Gaussian errors were added to daily rainfall and potential evapotranspiration during the simulation period from 2003 to 2021. The uncertainty range of rainfall is often chosen as $(0-15\%) \times R_t$ (Weerts & El Serafy, 2006). Here the standard deviation of random rainfall error was set as $15\% \times R_t$. The perturbation of evapotranspiration followed Plaza Guingla et al. (2013) where a $30\% \times Pev_t$ standard deviation was used.

Although this study primarily focuses on synthetic experiments, we aim to adapt the framework to accommodate the assimilation of real-world data for further research. Hence, the data assimilation frequency was set to be identical to the frequency of the real concentration measurements.

Once the simulation results are obtained as synthetic truth, the measurement errors should be added to observable states to simulate measurements as shown in equation 12 and equation 13 . The standard deviations of Gaussian measurement error are selected as 10% of LPR_t and C_t, respectively.

All the errors are presented in Table 1. It is worth emphasizing that although we try to simulate the actual case in the synthetic experiment, the artificial truth is only trying to approach the natural world in the context of a proof-of-concept study (Matgen et al., 2010).

Table 1. Standard deviation of Gaussian random errors for truth generation

Variables	R	Pev	v_{ini}	c_{ini}
Standard deviation	$0.15 \times R_t$	$0.3 \times Pev_t$	$0.1 \times v_{ini}$	$0.1 \times c_{ini}$

v_{ini} and c_{ini} represent all the initial volume and concentration states in the model.

2.6 Ensemble generation performance control

The performance of DA relies on the appropriate representation of uncertainties in the prediction. More specifically, the model error in equation 1 should make the spread of generated ensembles realistic compared to real measurements. Following the method proposed by De Lannoy et al. (2006), the ensemble spread($ensp_t$), the mean square error(mse_t), and the ensemble skill($ensk_t$) are calculated as:

$$ensp_t = \frac{1}{N}\sum_{i=1}^{N}(y_t^i - \overline{\boldsymbol{y}_t})^2 \tag{14}$$

$$mse_t = \frac{1}{N}\sum_{i=1}^{N}(y_t^i - y_{mea_t})^2 \tag{15}$$

$$ensk_t = (\overline{\boldsymbol{y}_t} - y_{mea_t})^2 \tag{16}$$

N, i, t, y, y_{mea} represent ensemble size, ith ensemble number, assimilation time step, simulated observable states, and assimilated measurements, respectively. According to De Lannoy et al. (2006), to ensure the generated ensembles' statistical accuracy, the following requirements should be considered:

$$\frac{< ensk >}{< ensp >} \approx 1 \tag{17}$$

<> means the average over the simulation time range. More specifically, a value larger than 1 indicates insufficient ensemble spread, while a value smaller than 1 indicates excessive spread. If the truth is indistinguishable from a member of the ensemble, the following equation should be true(De Lannoy et al., 2006):

$$\frac{< \sqrt{ensk} >}{< \sqrt{mse} >} \approx \sqrt{\frac{N+1}{2N}} \tag{18}$$

When both leachate production rate and concentration measurements are assimilated, we need a sufficiently large ensemble spread in the simulated output. This is achieved by manually optimizing the standard deviations of model error. Firstly we obtained the model error for the cover layer water storage using an interval search to get an appropriate spread in leachate production rate simulations. If the spread for concentration states is not sufficient or excessive with the chosen model error, we adjust the initial uncertainty range for the concentration states. Using this approach allows us to obtain a good ensemble spread for concentration states while not making the spread in leachage production excessive.

2.7 Implementation procedure

Based on the theory and model characteristics, the implementation of sequential importance resampling in this coupled TTD model is as follows:

1. Initialization: from the model calibration results, we take one parameter set and initial states in 2003. The initial samples are sampled from Gaussian distributions where the means are the optimized initial values. Initially, the corresponding percentiles of standard deviations in Gaussian distributions are set to be the same as the ones used in the generation of synthetic initial states (see table 1). Subsequently, the standard deviations undergo adjustment to meet the ensemble spread criteria, as is discussed in section 3.1. With a warm-up simulation, the samples are propagated to the starting date of data assimilation on the 19th June 2012, a time step 7 days earlier than the first measurement date. The reason to perform this warm-up propagation is that we need to build connections among waste body states. Otherwise, the time lag between bulk states and measurements will make the estimation unreliable.
2. Update step: all the particles are propagated to the next assimilation step with eqation 1, where $M(\cdot)$ indicates the coupled TTD model. The choice of model error is crucial for representing uncertainties and ensuring a good data assimilation technique performance. Most studies applying particle filter or ensemble Kalman filter choose to add a Gaussian random error to perturb forcing data, model states, and/or parameters (Weerts & El Serafy, 2006; Mattern et al., 2013; Vrugt et al., 2013; Tran et al., 2020). Considering the time lag issue, if we add independent model error to each state directly, the accumulation of errors of states like v_{bulk} will be huge after several years' lag. Therefore, we choose to add daily error to V_{cl}. The daily errors will be propagated to waste body states with time, which means we are adding correlated model errors to waste body states. Since the influence of error in V_{cl} on fast flow cells can be estimated by measurements very quickly, we can avoid adding too much unreasonable errors to old states like v_{bulk}. Additionally, this error choice maintains the total mass balance in all waste body volume states.
   No model error is introduced to the concentration states directly. Once the initial concentration values are determined, the concentration variation is assumed to be determined by volume states only.

3. Analysis step: the weights for particles are calculated by equation 7. Based on different assimilation strategies, we weigh the states differently. In a coupled assimilation scenario, the weights for volume w_v and concentration states w_c are calculated separately using their corresponding measurements. Both concentration and leachate volume are used to calculate w_m: $w_m = w_c * w_v$. Then w_m is normalized before estimating the mass states. If only concentration measurements are assimilated, all the model states are weighted based on the concentration measurements. When only LPR measurements are assimilated, the weights are used to estimate all states except concentration states.
4. Resampling step: this step is the same as the weights calculation, effective ensemble size N_v^{eff}, N_c^{eff} is computed according to equation 10. Then the corresponding particles will be resampled when N_t^{eff} is smaller than $N/2$. The mass states are recalculated from the resampled volume and concentration states, and the weights w_m are also updated with new w_v and w_c.
5. Iteration: all former steps after initialization are repeated until the last assimilation step.

2.8 Performance estimation

Besides the evolution of hidden states, the accuracy of state estimation results is evaluated with the temporal mean root-mean-square error, which is described in equation 19. The L indicates the number of assimilation time steps.

$$MRMSE = \frac{\sum_{t=1}^{L} \sqrt{\sum_{i=1}^{N} w_t^i (x_t^i - x_t^{truth})^2}}{L} \tag{19}$$

The prediction accuracy is also evaluated using a logarithmic form(η) proposed by (Ercolani & Castelli, 2017):

$$\eta = -\ln(1 - NSE) \tag{20}$$

where NSE is the Nash-Sutcliffe efficiency calculated as:

$$NSE = 1 - \frac{\sum_{t=1}^{T} (y_t - y_{mea_t})^2}{\sum_{t=1}^{T} (y_{mea_t} - \overline{y_{mea}})^2} \tag{21}$$

where y_{mea_t} are the measurements at time step t, y_t represents the model prediction, and the over bar means the average over time. The logarithmic scale allows dealing with high NSE values(close to 1). It tends to plus infinity when the observations and predictions achieve a perfect match. The reliability of ensemble prediction is not considered here because the model error is optimized to get reliable predictions.

2.9 Synthetic scenarios

Different synthetic scenarios are designed to test the application's feasibility. As shown in table 2, in total six scenarios are used to test the assimilation performance and get optimal assimilation strategy. Scenarios A, D follow the proposed coupled assimilation procedure described above. In other scenarios, only LPR or concentration measurements are assimilated. Scenarios D to F are similar to A to C but with the difference that we initialize the simulation with much smaller initial bulk volume values. These scenarios are used to test the influence of the baseflow function, which will be discussed in the following part. Two open-loop simulations are also performed to get reference results for scenarios $A - C$ and $D - E$. The open loop simulations have the same initial sample distributions and model errors as corresponding scenarios, but no measurements are assimilated to update model states. The related state estimation and prediction results of scenarios $B - C, E - F$ are provided in the supporting information.

Table 2. Synthetic scenarios

Scenario	Assimilate LPR	Assimilate C	Small initial V_{bulk}
A	Yes	Yes	No
B	Yes	No	No
C	No	Yes	No
D	Yes	Yes	Yes
E	Yes	No	Yes
F	No	Yes	Yes
$\text{OL}_{\text{A-C}}$	No	No	No
$\text{OL}_{\text{D-F}}$	No	No	Yes

3 Results and discussion

3.1 Ensemble generation

The appropriateness of ensemble generation and the generated initial particles on the starting date of data assimilation, which is the 19th of June, is verified using equations 17 and 18. Based on the results of a preliminary sensitivity analysis of ensemble size, all experiments use 10240 particles to ensure stable performance. The final choice of initialization, model errors and the corresponding ensemble generation skills are presented in table 3.

Table 3. Ensemble generation performance

Scenario	$M_{v_{bulk}}$	$\sigma_{v_{bulk}}$	$\sigma_{c_{bulk}}$	$\epsilon_{V_{cl}}$	$\frac{<ensk>}{<ensp>}_{LPR}$	$\frac{<\sqrt{ensk}>}{<\sqrt{mse}>}_{LPR}$	$\frac{<ensk>}{<ensp>}_{C}$	$\frac{<\sqrt{ensk}>}{<\sqrt{mse}>}_{C}$
A-C	4.067	0.100	0.130	0.0145	1.002	0.651	1.082	0.587
D-E	2.000	0.100	0.100	0.0135	0.998	0.624	1.013	0.583

Note. All the initial states in 2003 are sampled from Gaussian distributions $N(M, \sigma \times M)$. The distribution parameters are the same as truth generation if not explicitly defined in the table. $M_{v_{bulk}}$ represents the initial mean of bulk water storage. $\sigma_{v_{bulk}}$ and $\sigma_{c_{bulk}}$ refer to the standard deviation percentile of bulk water storage and chloride concentration, respectively. $\epsilon_{V_{cl}}$ shows the standard deviation percentile for model error added to cover layer water storage.

3.2 Assimilation performance

The assimilation performance of the method is evaluated using the proposed performance matrices (equation 19 - 21). The estimation and prediction results in different scenarios are compared to investigate the performance under different conditions in Table 4.

3.2.1 Estimation of hidden states

The estimated values for total water storage in the cover layer, chloride mass, water storage in the waste body are presented in Table 4. In addition, the results of average chloride concentration are presented to understand the state update process better. Although there is a small amount of chloride in the cover layer, it can be ignored compared with the amount in the waste body.

Table 4. MRMSE of estimated model states

State	$OL_{A\text{-}C}$	A	B	C	$OL_{D\text{-}F}$	D	E	F
$V_{cl}[m]$	7.92e-3	7.06e-3	7.36e-3	7.02e-3	6.12e-3	5.22e-3	5.41e-3	5.43e-3
$V_{wb}[m]$	0.636	0.577	0.590	0.609	0.296	0.187	0.198	0.226
$C_{wb}[g/m^3]$	258.422	83.996	264.225	87.850	197.498	52.667	183.845	58.087
$M_{wb}[g/m^2]$	1327.724	1273.604	1161.753	1388.788	640.975	310.564	482.107	388.053

3.2.1.1 Total water storage in cover layer

As shown in Table 4, the four MRMSE values for the storage in the cover layer (V_{cl}) in A-C and OL_{A-C} scenarios are similar. This observation is supported by the standard deviations of MRMSE, which are within a magnitude of $4 \times 10^{-3}m$. Similar estimation performance is observed in scenarios D-F and OL_{D-F}, where the standard deviations of MRMSE are within a magnitude of $3 \times 10^{-3}m$. The values of the standard deviations of RMSE are in the uploaded output file. All the scenarios, including open loop realizations in Figure 2, Figure 3 and Figure S1 - S4 (see the supporting information), show good consistency with actual states. This is caused by the buffering effect of the unsaturated soil model used to simulate V_{cl}. When saturation is high, infiltration to the waste body will be high as well. If no model error or forcing data errors were added, the V_{cl} starting with different values would converge to a same value after a period of time. The random model error added during DA is the main source for the uncertainty in V_{cl}. Figure 2 and Figure 3 show that the uncertainty ranges in scenarios A and D vary with time but within a limited bandwidth because no decreasing trend exists. Similar results are observed in Figure S1 - S4 in the supporting information when only leachate production rate or chloride concentration measurements are assimilated. The estimates during wet periods are better than those during dry periods. This is most likely caused by the limited information content of V_{cl} in the outflow when there is only little infiltration from cover layer, and the outflow is mainly dominated by baseflow from the waste body.

3.2.1.2 Total water storage in waste body

Scenarios A - C are initialized with high values for initial bulk water storage. Scenario B has similar waste body water storage (V_{wb}) estimation results as scenario A because of the same assimilation procedure for volume states (see Figure 4, Figure S5 in the supporting information). As shown in Figure 4, S5 and S6 (see supporting information), the mean estimation shows no noticeable improvement for the whole period in scenarios A, B and C. When the model is initialized with a lower value for the initial bulk water storage in scenarios D, E and F, the behaviour is quite different. As shown in Figure 5, S7 and S8 (see supporting information), the biases in the total water storage are corrected by assimilation of new measurements compared with the large bulk water storage scenarios. In scenarios D and E, the particles finally converge to true values, and the uncertainties are much smaller compared with the open-loop results. The MRMSE values in Table 4 also show greater improvement compared with large storage scenarios.

The difference in assimilation performance of two different initial values in water storage is caused by the baseflow function. As discussed in the time lag issue, we can only estimate hidden states if the measurements are sensitive to their variations. Figure 6 shows the baseflow function, which links the bulk water storage to generated baseflow volume. Bulk water storage takes up a large part of the total water storage in the waste body. Hence, the estimation of bulk water storage is crucial for V_{wb} estimation. As we can see, baseflow is only sensitive to bulk water storage variation when bulk water storage falls between 0 and 2 meters. In addition, Figure 7 shows the travel time distribution of baseflow. Almost all the generated baseflow is distributed to the oldest cell. It means the information of any change

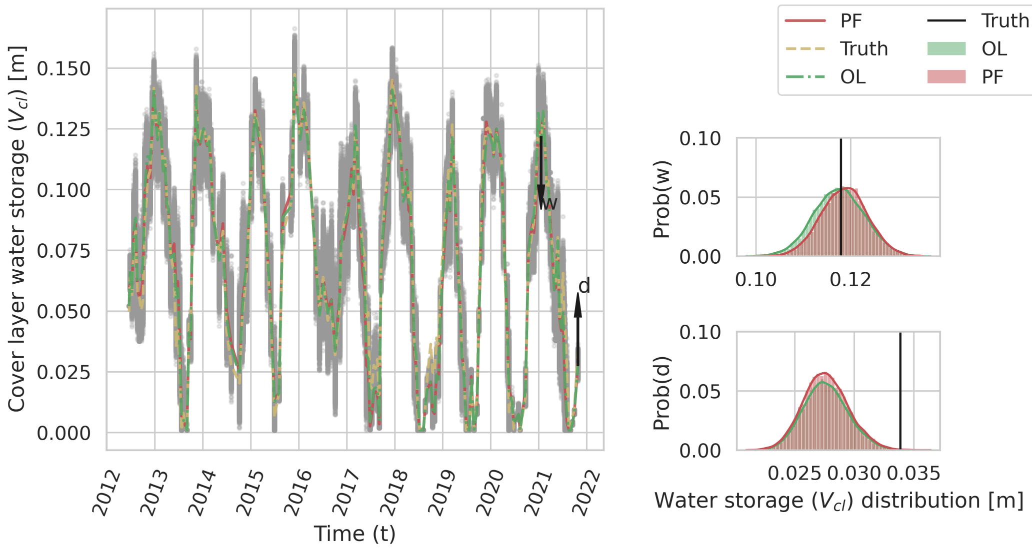

Figure 2. Water storage in the cover layer (scenario A). The red line represents the mean estimation of the particle filter. The green and yellow lines represent the open loop results and synthetic truth, respectively. The individual particles are shown as grey points. The two black arrows point to the wet and dry period during the assimilation process, with corresponding probabilities plotted. The black vertical lines in the probability histograms are the truth at specific time steps.

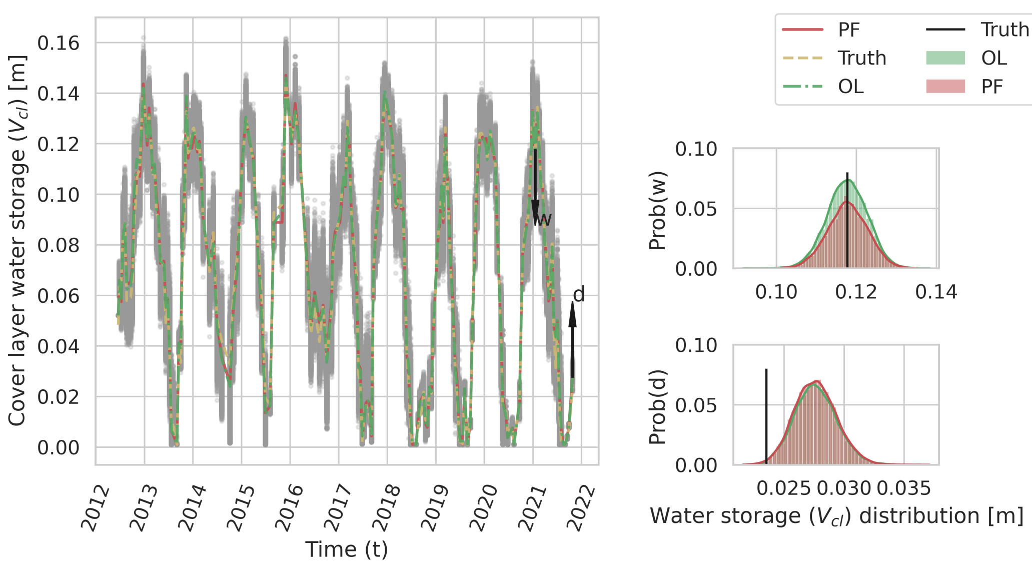

Figure 3. Water storage in the cover layer (scenario D). Colors of lines as in Figure 2.

in bulk storage takes five years before it is observed in simulated leachate production rates. According to the synthetic truth, the bulk water storage five years before the last measurement in scenarios A-C is around 2.18m. Obviously, the information in the measurements to quantify bulk water storage is limited. Lower values of the bulk water storage allow the baseflow to reduce during the simulation time span. As a consequence, measured leachate production rates contain information on this reduced water storage because of lower baseflow values. This improves the estimate of bulk water storage and V_{wb}, leading to lower uncertainty.

Figure S8 (see supporting information) also shows that when the information content of the measurements is high, the concentration measurements can be used to estimate V_{wb}. Another influencing factor of the uncertainty quantification capacity is the measurement error. While the measurement errors are small, it can detect smaller baseflow changes. For example, the bulk water content will still influence the baseflow when it varies between 2 and 3 meters. When the measurement error is relatively large compared to the corresponding baseflow variation, most of the particle sets in this range will have close wights as they all give similar baseflow output. As shown in Figure 4, only large and small particle sets are discarded with assimilation. Also, the MRMSE values in Table 4 show slight improvement compared with open-loop results. To further quantify the uncertainty and correct the bias in mean estimation, the time series of measured leachate production rates should be long enough to capture the effect of reducing bulk water storage values in the sensitive range.

Compared with scenario D, the mean estimation in scenario F takes more time to correct the bias. And the final uncertainty estimation is not as good as scenario D. It is because the weights in scenario F are calculated using concentration measurements, which are also influenced by mass states. The particles with the wrong volume and mass values but correct concentration values are also considered with high probability. This is also reflected in Table 4, where the MRMSE of scenario F is larger than D and E.

In scenarios A, B and C, the posterior distributions in wet periods are close to the ones obtained during dry periods. This means that the estimation results of V_{wb} are stable during the last wet-dry cycle. However, in scenarios D and E, the posterior distributions in dry periods still change compared with wet periods. This indicates that the measurements in the last cycle still contain new information content which are being assimilated to reduce the uncertainty.

3.2.1.3 Average chloride concentration in waste body

Estimation of the average chloride concentration in the waste body is another case where the 'history' is required. All available measurements are linked to the first cell only. Nevertheless, the estimation of the average concentration becomes possible because of the 'history' connection between cells and bulk. As shown in Figures 8, Figure 9, S10 and S12 (see supporting information), the uncertainties in average concentration are reduced compared with the open-loop results. Irrespective of the sensitivity of the baseflow to bulk water storage variation, the chloride in waste body bulk is the source of chloride in the mobile cells, which enables us to use concentration measurements to estimate the average concentration.

As shown in Figures S9 and S11 (see supporting information), the estimations of average concentration are poor when only Leachage Production Rate (LPR) measurements are assimilated. More specifically, the posterior distributions and mean estimations are very close to open-loop results. Although the volume states can be quantified in scenario D, it doesn't help reduce the uncertainty range in average concentration. It is worth noting that when only concentration states are assimilated in scenarios F, Figure S12 shows larger uncertainty but slightly better mean estimation results compared with corresponding scenario D, where both measurements are assimilated. Although assimilation using only LPR measurements does not really influence the estimation of the concentration state, all the volume and mass state combinations with correct concentration values but wrong volume values will be discarded in scenarios D. The impact on the estimation step is minimal while

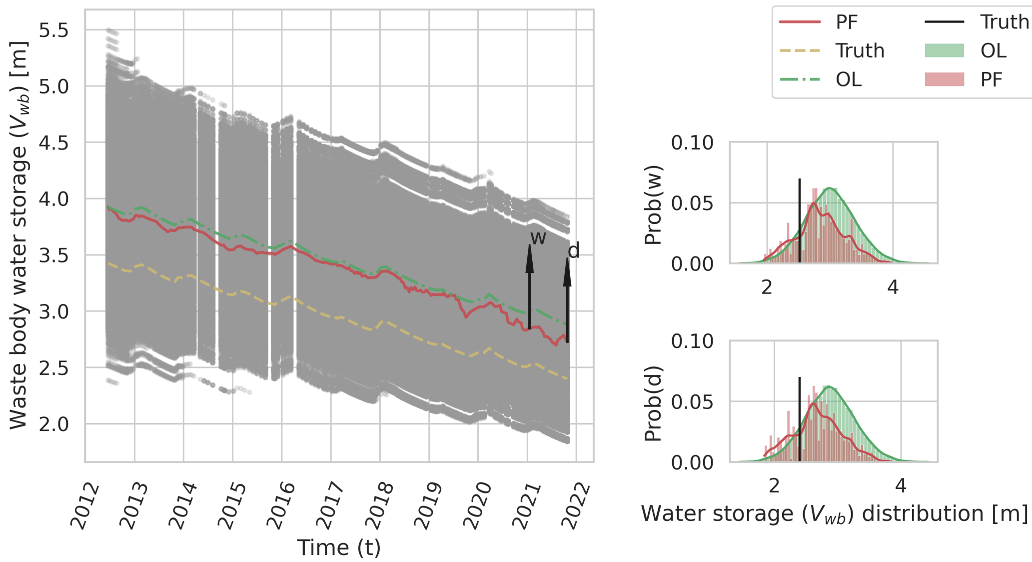

Figure 4. Water storage in the waste body in scenario A. Colors of lines as in Figure 2.

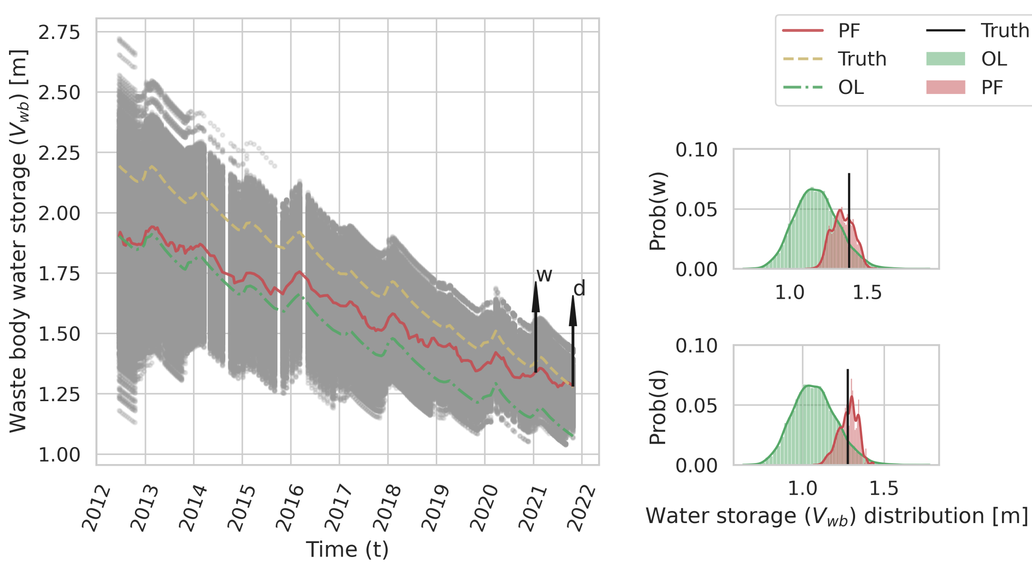

Figure 5. Water storage in the waste body in scenario D. Colors of lines as in Figure 2.

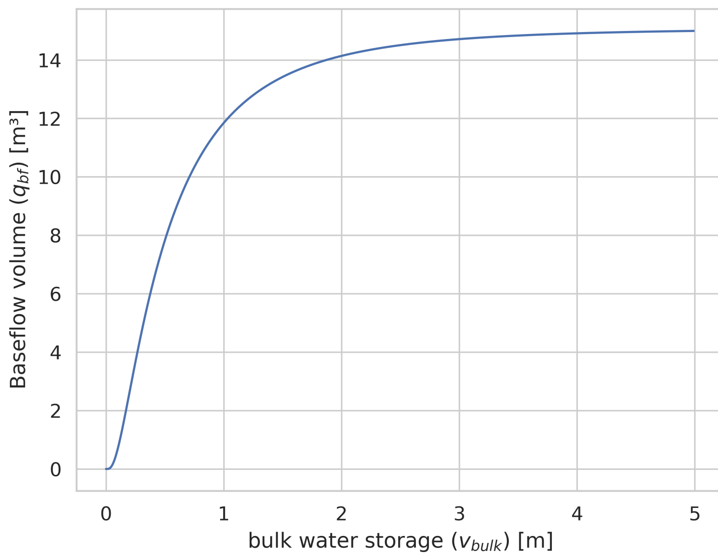

Figure 6. Baseflow change with bulk water storage variation

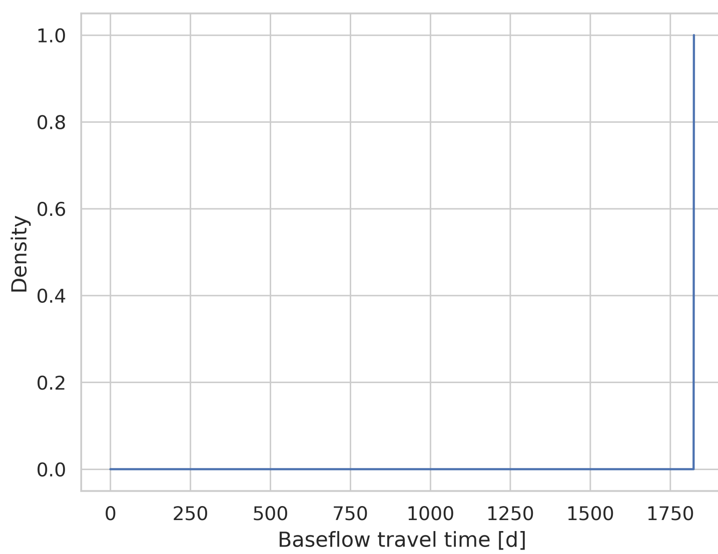

Figure 7. Baseflow travel time distribution

the diversity in predicted concentration samples is reduced because the prediction is based on both concentration and water storage states. Overall, the assimilation of concentration states helps quantify the uncertainty in concentration states.

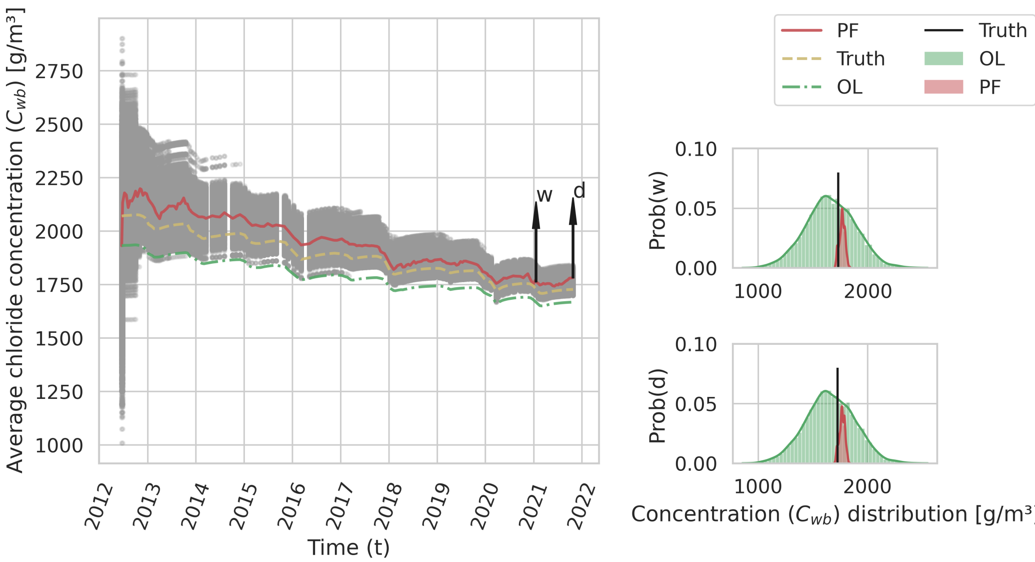

Figure 8. Average concentration in the waste body in scenario A. Colors of lines as in Figure 2.

3.2.1.4 Total chloride mass in waste body

The total chloride mass in the waste body is calculated from the estimated water volume and concentration states. The uncertainty reduction in either volume states or concentration states reduces the uncertainty of mass states. On the other hand, bias in estimation of volume or concentration states can result in bias in mass estimation even if the other estimation is perfect.

As shown in Table 4, when initial bulk water storage is small, all the synthetic experiments have better MRMSE results than open-loop simulations. Assimilating both measurements achieves the best estimation results. In contrast, when the initial bulk storage is high, the MRMSE remains relatively high after assimilation. Starting with different initial bulk water content, scenario B performs best among scenarios A-C while scenario E is the worst among scenarios D-F. The MRMSE result for scenario B is unusually small because it yields a higher estimation of volume and a lower estimation of average concentration states. This, in turn, results in a better mean estimation of mass states.

Figures 10 and 11 show the evolution of M_{wb} estimation when both measurements are assimilated. Scenario A shows slightly reduced posterior uncertainty, which indicates insufficient information in flow measurements. As a comparison, scenario D gains much more improvement in posterior distributions, which is because of the good estimations of both volume and concentration states. As discussed in section 3.2.1.2, the difference is because of the different sensitivities of baseflow to bulk storage volume. Similarly, the improvement from the wet period to the dry period in scenario D is caused by the information content in LPR measurements.

When only LPR measurements are assimilated, there is little improvement in mass estimation if the baseflow is not sensitive to bulk storage change, as shown in Figure 13 (see supporting information). In scenario E, as shown in Figure S15 (see supporting information), the uncertainty range of M_{wb} is reduced, and the mean estimation accuracy is better than open-loop results. However, we cannot make a conclusion that LPR measure-

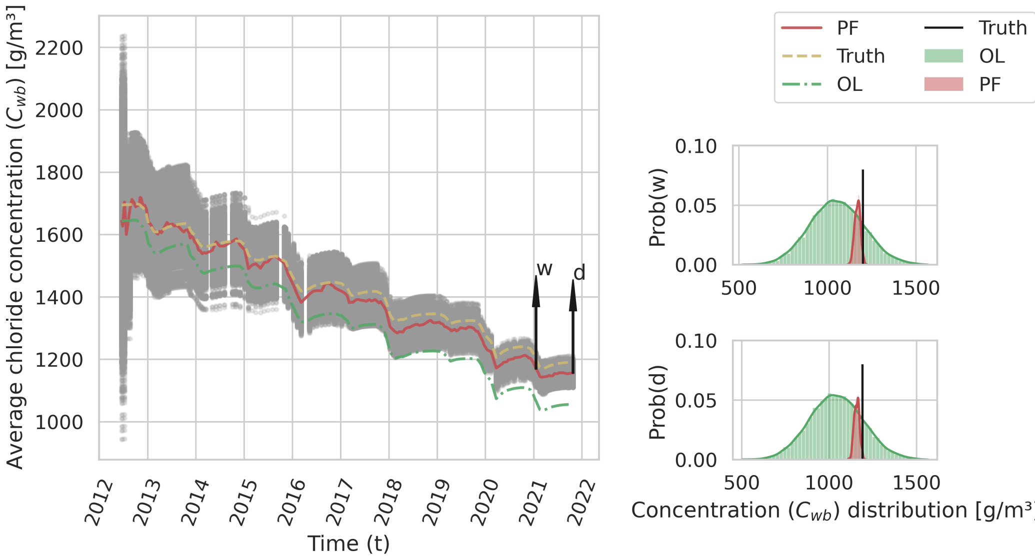

Figure 9. Average concentration in the waste body in scenario D. Colors of lines as in Figure 2.

ment assimilation is sufficient to quantify the uncertainty in total chloride mass. Because the estimation of M_{wb} is also controlled by the initialization of concentration states. If the generated initial concentration states are biased, there is always a risk of biased estimation of M_{wb}.

In scenario C (see S14 in the supporting information), reduced uncertainty is observed, but the mean estimations are not better than open-loop results. However, scenario F shows much better mean estimation convergence compared with open-loop results. The difference between scenarios C and F is also mainly because of the different estimation performance of V_{wb}.

Following the conclusion from volume and concentration estimations, solely assimilating LPR measurements is not sufficient for emission potential estimation. When the sensitivity of baseflow to bulk storage is high, we can use concentration measurements solely to estimate the M_{wb}. Assimilating both measurements achieves the best performance in the sense of both mean estimation and uncertainty reduction.

3.2.2 Prediction performance

Table 5. Prediction performance

	Scenario	$OL_{A\text{-}C}$	A	B	C	$OL_{D\text{-}F}$	D	E	F
LPR	$MRMSE[m^3]$	3.332	2.360	2.444	2.555	3.116	2.178	2.248	2.465
	NSE	0.940	0.944	0.944	0.944	0.948	0.950	0.950	0.954
	η	2.805	2.892	2.893	2.884	2.955	2.989	2.988	3.071
C	$MRMSE[g/m^3]$	186.728	66.377	178.000	68.791	138.320	47.741	122.924	50.743
	NSE	0.798	0.878	0.808	0.874	0.866	0.918	0.881	0.914
	η	1.600	2.101	1.653	2.074	2.009	2.497	2.126	2.458

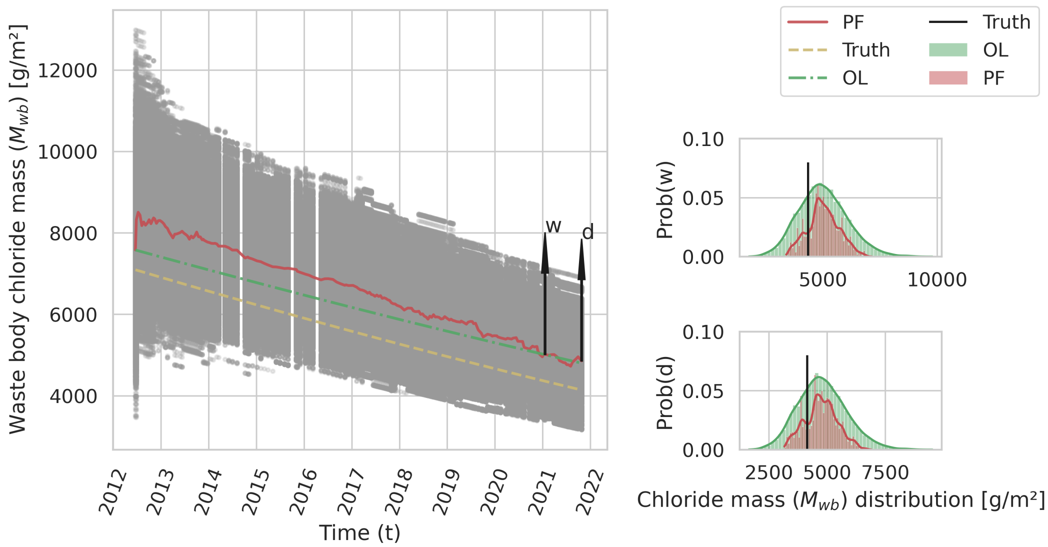

Figure 10. Chloride mass in the waste body in scenario A. Colors of lines as in Figure 2.

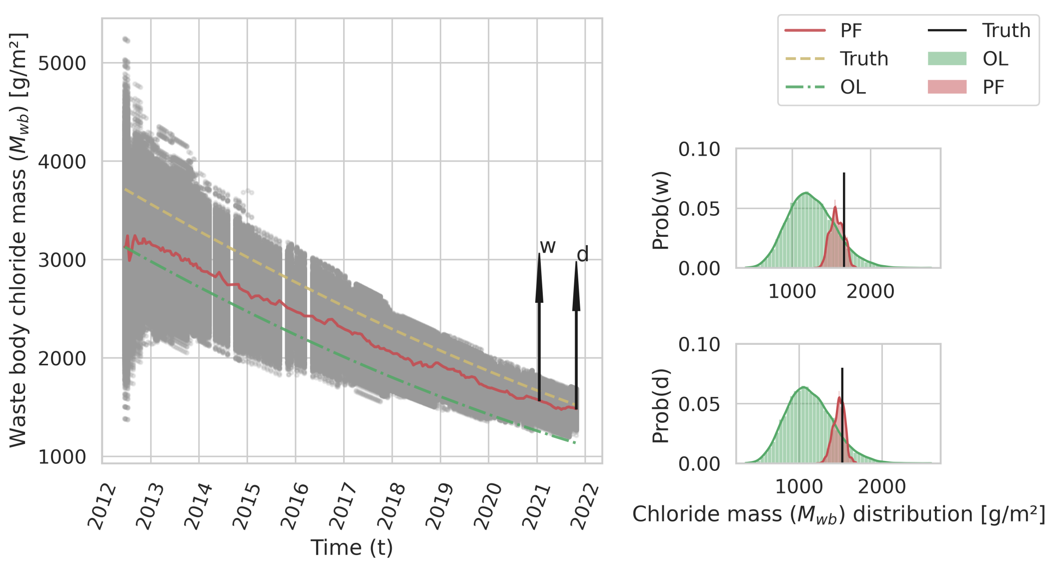

Figure 11. Chloride mass in the waste body in scenario D. Colors of lines as in Figure 2.

3.2.2.1 Leachate production rates

Table 5 shows the metrics we use to quantify the quality of the predicted states. All six scenarios have smaller MRMSE values and greater η values compared with the corresponding open-loop simulations. This indicates reduced prediction uncertainty and improved accuracy. However, the η values of three scenarios with the same initial bulk storage are very close, and the difference between similar scenarios is small. This is also observed in Figures 12, 13 and S17-S20 in the supporting information, where the open-loop simulations also have good LPR prediction performance.

As discussed in section 3.2.1.1, the estimation of cover layer water storage has a relatively good consistency with the truth in all scenarios which guarantees the accuracy of LPR prediction, especially in wet periods where infiltration from the cover layer takes up most of the outflow. Additionally, when the bulk storage in the waste body, v_{bulk}, reduces below 1 m (see Figure 6), the baseflow magnitude will reduce significantly. Under such conditions baseflow will show a large sensitivity to infiltration from the cover layer reaching the bulk storage.

Although scenario D, as shown in Figure 5, has a better waste body water storage estimation than scenario F (see Figure S8 in supporting information), scenario F has a higher η value compared with scenario D. This is because more particles smaller than one meter remain in the posterior distribution of scenario F, which is important to catch the effect of change in bulk storage on the base flow. Also, η is calculated using synthetic measurements which contain measurement error. There are some values smaller than truth in the dry period which cannot be covered by true v_{bulk} values. This can also be observed by comparing Figure 13 and S20 (see supporting information), where more low LPR measurements are covered in scenario F.

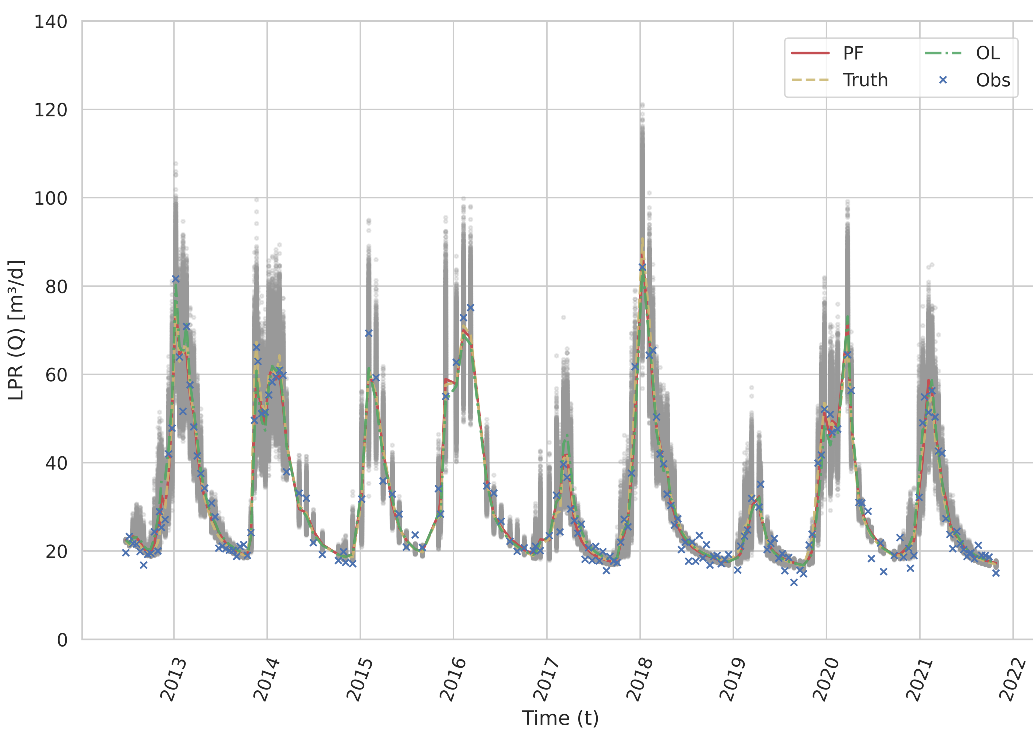

Figure 12. LPR prediction in scenario A. The blue crosses indicate the behaviour of synthetic measurements. Colors of lines as in Figure 2.

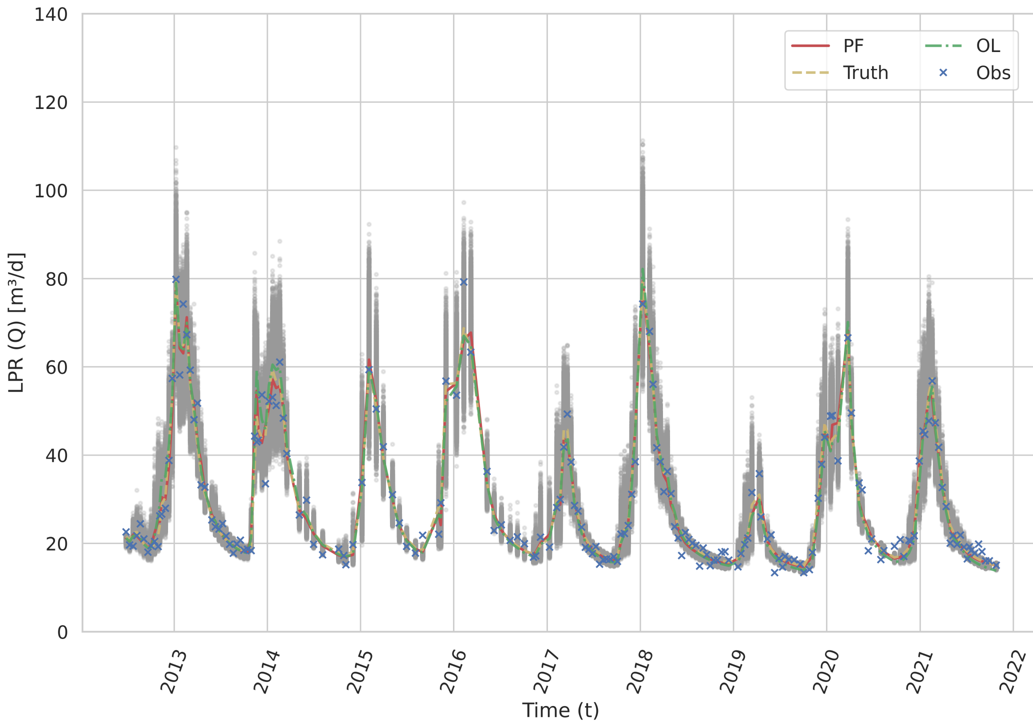

Figure 13. LPR prediction in scenario D. Colors of lines and crosses as in Figure 12.

3.2.2.2 Chloride concentrations

As shown in Table 5, when concentration measurements are assimilated in scenarios A, C, D and F, the values of prediction accuracy η improve significantly compared with open-loop realizations. As shown in Figure 14, Figure 15, S22 and S24 (see supporting information), the red lines follow the yellow truth quite well. When only LPR measurements are assimilated, we also observe the reduction of MRMSE and improvement of η. However, compared with the scenarios assimilating concentrations, the improvement is very small. The uncertainty in concentrations is only controlled by the assigned uncertainty when calculating the initial concentration states. Filtering the water storage states does not introduce new information to the concentration states. If there are infinite random particles, we expect to see an identical prediction as in the open-loop simulations.

4 Summary and Conclusions

This work presents a weakly coupled particle filter framework to assimilate leachate production rates and chloride concentrations with the aim to estimate the emission potential of landfill waste bodies. The emission potential in this paper is defined as the mass of leachable chloride present in the waste body. A concentration-coupled travel time distribution model was used as a forward model for data assimilation. Synthetic experiments were performed to investigate the feasibility of state estimation and improving prediction. Six scenarios were developed to investigate the best assimilation strategy. Two synthetic measurement data sets were generated with the same forward model using different initial bulk water content values under identical meteorological forcing conditions. On each synthetic data set, three types of Data Assimilation were carried out: DA using both Leachate Production Rate (LPR) and concentration measurements and DA using only LPR or concentration measurements.

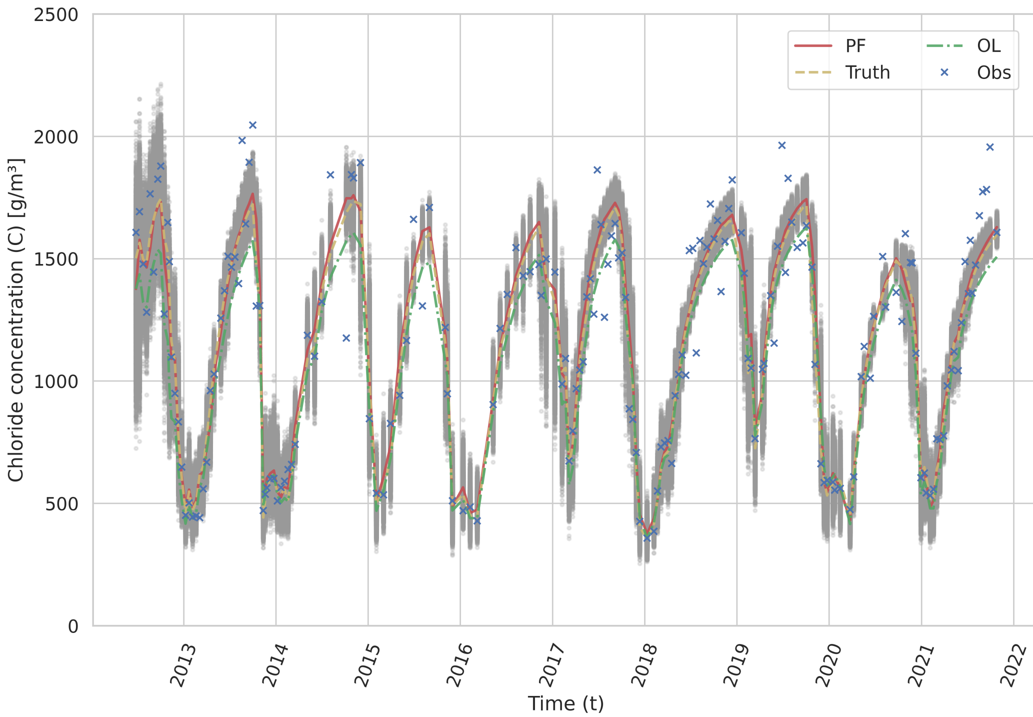

Figure 14. Concentration predication in scenario A. Colors of lines and crosses as in Figure 12.

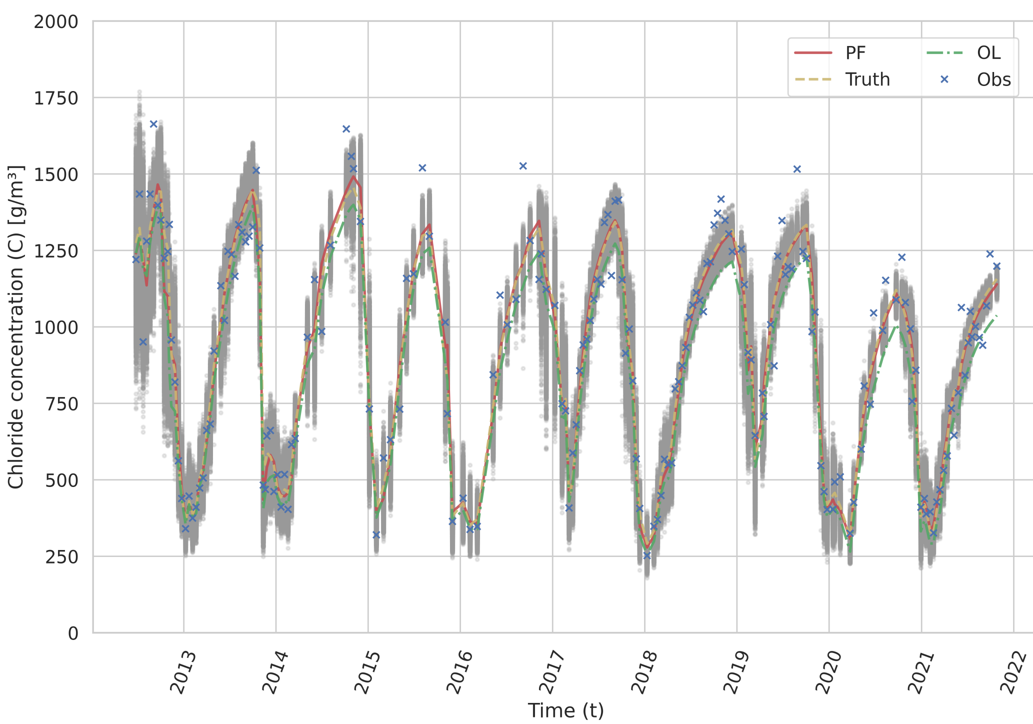

Figure 15. Concentration predication in scenario D. Colors of lines and crosses as in Figure 12.

The results from the different scenarios show that sensitivity of baseflow to bulk water storage volume plays a vital role in controlling the assimilation performance. When the bulk water storage is within the range where its change has limited influence on baseflow, assimilating measurements cannot reduce the uncertainties in waste body water storage.

The results also indicate that the improvement in the estimation of cover layer water storage is limited as the open-loop realizations already have good consistency with synthetic truth. Assimilating concentration measurements improves the estimation of average concentration states in the waste body. It also benefits the estimation of water storage states as the concentration states are coupled to the water balance model. However, assimilation with concentration measurements alone reduces the convergence of water storage estimation in comparison with assimilating both LPR and concentration measurements. In contrast, assimilating LPR helps quantify the uncertainty in water storage states in the waste body, while it doesn't reduce the uncertainties in concentration states. The proposed coupled assimilation method leads to good estimation results in both water storage and concentration states.

The estimation of emission potential heavily relies on accurate estimation of the total water storage and concentration states within the waste body. Reducing uncertainties in volume or concentration states leads to a reduction in uncertainties associated with the emission potential. Therefore, improving the estimation of volume and concentration states directly contributes to minimizing uncertainties in emission potential. The results show the uncertainty is reduced in all the tested scenarios where the baseflow is sensitive to bulk storage change.

The LPR prediction improvement after assimilation is not significant, as the open-loop realizations also have good predictions. In contrast, the concentration predictions improved considerably when the chloride concentration measurements were assimilated.

Overall, the results of this study indicate that the proposed coupled assimilation procedure can be used to estimate total water storage and chloride mass in the waste body. As such, Data Assimilation is demonstrated to be a viable approach to quantify the emission potential of landfill waste bodies. The assimilation of LPR rates helped improve the accuracy of the estimation of total water storage, V_{wb}, compared to assimilating concentrations alone. The gap between volume states and mass states is filled by concentration assimilation. Future studies will focus on quantifying the uncertainty caused by model parameters, which, for example, determine the sensitivity of baseflow to bulk water storage volume.

5 Data Availability Statement

The data and codes used in this paper are available at link: `https://data.4tu.nl/private_datasets/DdrykoWpu1L5rI7SIOYpr9LFly0MiLtcXbMEeMmvIDk`.

Acknowledgments

This research is part of the CURE project supported by the Dutch National Science Foundation (NWO) under project no. OCENW.GROOT.2O19.O92. The research is also supported by the Dutch Sustainable Landfill Foundation via the iDS project. The authors also express appreciation to the support from Chinese Scholarship Council (No. 201906090271).

References

Abbaszadeh, P., Moradkhani, H., & Daescu, D. N. (2019). The quest for model uncertainty quantification: A hybrid ensemble and variational data assimilation framework. *Water resources research*, *55*(3), 2407–2431.

Arulampalam, M. S., Maskell, S., Gordon, N., & Clapp, T. (2002). A tutorial on particle filters for online nonlinear/non-gaussian bayesian tracking. *IEEE Transactions on signal processing*, *50*(2), 174–188.

Brand, E. (2014). Development of emission testing values to assess sustainable landfill management on pilot landfills: Phase 2: Proposals for testing values.

Carrassi, A., Bocquet, M., Bertino, L., & Evensen, G. (2018). Data assimilation in the geosciences: An overview of methods, issues, and perspectives. *Wiley Interdisciplinary Reviews: Climate Change*, *9*(5), e535.

De Lannoy, G. J., Houser, P. R., Pauwels, V. R., & Verhoest, N. E. (2006). Assessment of model uncertainty for soil moisture through ensemble verification. *Journal of Geophysical Research: Atmospheres*, *111*(D10).

Djurić, P., Kotecha, J., Zhang, J., Huang, Y., & Bugallo, M. (2003). Particle filters. *IEEE Signal Processing Magazine*, 19–38.

Duurzaam stortbeheer. (2023). *English page.* (Available at: `https://duurzaamstortbeheer.nl/english-page/`)

El Gharamti, M., Hoteit, I., & Valstar, J. (2013). Dual states estimation of a subsurface flow-transport coupled model using ensemble kalman filtering. *Advances in water resources*, *60*, 75–88.

Ercolani, G., & Castelli, F. (2017). Variational assimilation of streamflow data in distributed flood forecasting. *Water Resources Research*, *53*(1), 158–183.

Evensen, G. (2003). The ensemble kalman filter: Theoretical formulation and practical implementation. *Ocean dynamics*, *53*, 343–367.

Fatoba, J. O., Eluwole, A. B., Sanuade, O. A., Hammed, O. S., Igboama, W. N., & Amosun, J. O. (2021). Geophysical and geochemical assessments of the environmental impact of abule-egba landfill, southwestern nigeria. *Modeling Earth Systems and Environment*, *7*, 695–701.

Fellner, J., & Brunner, P. H. (2010). Modeling of leachate generation from msw landfills by a 2-dimensional 2-domain approach. *Waste Management*, *30*(11), 2084–2095.

Fellner, J., Döberl, G., Allgaier, G., & Brunner, P. H. (2009). Comparing field investigations with laboratory models to predict landfill leachate emissions. *Waste Management*, *29*(6), 1844–1851.

Gelsinari, S., Doble, R., Daly, E., & Pauwels, V. R. (2020). Feasibility of improving groundwater modeling by assimilating evapotranspiration rates. *Water Resources Research*, *56*(2), e2019WR025983.

Grugnaletti, M., Pantini, S., Verginelli, I., & Lombardi, F. (2016). An easy-to-use tool for the evaluation of leachate production at landfill sites. *Waste management*, *55*, 204–219.

Gworek, B., Dmuchowski, W., Koda, E., Marecka, M., Baczewska, A. H., Brągoszewska, P., ... Osiński, P. (2016). Impact of the municipal solid waste łubna landfill on environmental pollution by heavy metals. *Water*, *8*(10), 470.

Hol, J. D., Schon, T. B., & Gustafsson, F. (2006). On resampling algorithms for particle filters. In *2006 ieee nonlinear statistical signal processing workshop* (pp. 79–82).

Janjić, T., Bormann, N., Bocquet, M., Carton, J., Cohn, S. E., Dance, S. L., ... others (2018). On the representation error in data assimilation. *Quarterly Journal of the Royal Meteorological Society*, *144*(713), 1257–1278.

Kalman, R. E. (1960, 03). A New Approach to Linear Filtering and Prediction Problems. *Journal of Basic Engineering*, *82*(1), 35-45. Retrieved from `https://doi.org/10.1115/1.3662552` doi: 10.1115/1.3662552

Kattenberg, W., & Heimovaara, T. (2011). Policy process of allowing research pilots for sustainable emission reduction at landfills in the netherlands. In *Proceedings sardinia.*

Laloyaux, P., Balmaseda, M., Dee, D., Mogensen, K., & Janssen, P. (2016). A coupled data assimilation system for climate reanalysis. *Quarterly Journal of the Royal Meteorological Society*, *142*(694), 65–78.

Laner, D., Fellner, J., & Brunner, P. H. (2011). Future landfill emissions and the effect of final cover installation–a case study. *Waste management*, *31*(7), 1522–1531.

Li, Y., Ryu, D., Western, A. W., & Wang, Q. (2013). Assimilation of stream discharge for flood forecasting: The benefits of accounting for routing time lags. *Water resources research*, *49*(4), 1887–1900.

Liu, Y., & Gupta, H. V. (2007). Uncertainty in hydrologic modeling: Toward an integrated data assimilation framework. *Water resources research*, *43*(7).

Liu, Y., Weerts, A., Clark, M., Hendricks Franssen, H.-J., Kumar, S., Moradkhani, H., ... others (2012). Advancing data assimilation in operational hydrologic forecasting: progresses, challenges, and emerging opportunities. *Hydrology and earth system sciences*, *16*(10), 3863–3887.

Matgen, P., Montanari, M., Hostache, R., Pfister, L., Hoffmann, L., Plaza, D., ... Savenije, H. (2010). Towards the sequential assimilation of sar-derived water stages into hydraulic models using the particle filter: proof of concept. *Hydrology and Earth System Sciences*, *14*(9), 1773–1785.

Mattern, J. P., Dowd, M., & Fennel, K. (2013). Particle filter-based data assimilation for a three-dimensional biological ocean model and satellite observations. *Journal of Geophysical Research: Oceans*, *118*(5), 2746–2760.

McMillan, H., Hreinsson, E., Clark, M., Singh, S., Zammit, C., & Uddstrom, M. (2013). Operational hydrological data assimilation with the recursive ensemble kalman filter. *Hydrology and Earth System Sciences*, *17*(1), 21–38.

Moore, R. (1985). The probability-distributed principle and runoff production at point and basin scales. *Hydrological Sciences Journal*, *30*(2), 273–297.

Ng, G.-H. C., McLaughlin, D., Entekhabi, D., & Scanlon, B. (2009). Using data assimilation to identify diffuse recharge mechanisms from chemical and physical data in the unsaturated zone. *Water resources research*, *45*(9).

Noh, S. J., Rakovec, O., Weerts, A. H., & Tachikawa, Y. (2014). On noise specification in data assimilation schemes for improved flood forecasting using distributed hydrological models. *Journal of hydrology*, *519*, 2707–2721.

Noh, S. J., Tachikawa, Y., Shiiba, M., & Kim, S. (2013). Ensemble kalman filtering and particle filtering in a lag-time window for short-term streamflow forecasting with a distributed hydrologic model. *Journal of Hydrologic Engineering*, *18*(12), 1684–1696.

Pantini, S., Verginelli, I., & Lombardi, F. (2014). A new screening model for leachate production assessment at landfill sites. *International Journal of Environmental Science and Technology*, *11*, 1503–1516.

Penny, S., Bach, E., Bhargava, K., Chang, C.-C., Da, C., Sun, L., & Yoshida, T. (2019). Strongly coupled data assimilation in multiscale media: Experiments using a quasi-geostrophic coupled model. *Journal of Advances in Modeling Earth Systems*, *11*(6), 1803–1829.

Penny, S. G., & Hamill, T. M. (2017). Coupled data assimilation for integrated earth system analysis and prediction. *Bulletin of the American Meteorological Society*, *98*(7), ES169–ES172.

Plaza Guingla, D. A., De Keyser, R., De Lannoy, G. J., Giustarini, L., Matgen, P., & Pauwels, V. R. (2013). Improving particle filters in rainfall-runoff models: Application of the resample-move step and the ensemble gaussian particle filter. *Water Resources Research*, *49*(7), 4005–4021.

Royal Dutch Meteorological Institute (KNMI). (2023). *KNMI Climate Data.* `https://www.daggegevens.knmi.nl/klimatologie/daggegevens`.

São Mateus, M. d. S. C., Machado, S. L., & Barbosa, M. C. (2012). An attempt to perform water balance in a brazilian municipal solid waste landfill. *Waste Management*, *32*(3), 471–481.

Shockley, E. (2020). *A python implementation of the mt-dream(zs) algorithm from laloy* *and vrugt 2012.* Online. Retrieved from `https://github.com/LoLab-MSM/PyDREAM`

Smith, P. J., Fowler, A. M., & Lawless, A. S. (2015). Exploring strategies for coupled 4d-var data assimilation using an idealised atmosphere–ocean model. *Tellus A: Dynamic Meteorology and Oceanography*, *67*(1), 27025.

Tardif, R., Hakim, G. J., & Snyder, C. (2015). Coupled atmosphere-ocean data assimilation experiments with a low-order model and cmip5 model data. *Climate Dynamics*, *45*, 1415–1427.

Tran, V. N., Dwelle, M. C., Sargsyan, K., Ivanov, V. Y., & Kim, J. (2020). A novel modeling framework for computationally efficient and accurate real-time ensemble flood forecasting with uncertainty quantification. *Water Resources Research*, *56*(3), e2019WR025727.

Van Leeuwen, P. J. (2009). Particle filtering in geophysical systems. *Monthly Weather Review*, *137*(12), 4089–4114.

Vrugt, J. A. (2016). Markov chain monte carlo simulation using the dream software package: Theory, concepts, and matlab implementation. *Environmental Modelling & Software*, *75*, 273–316.

Vrugt, J. A., ter Braak, C. J., Diks, C. G., & Schoups, G. (2013). Hydrologic data assimilation using particle markov chain monte carlo simulation: Theory, concepts and applications. *Advances in Water Resources*, *51*, 457–478.

Weerts, A. H., & El Serafy, G. Y. (2006). Particle filtering and ensemble kalman filtering for state updating with hydrological conceptual rainfall-runoff models. *Water resources research*, *42*(9).

Yang, N., Damgaard, A., Kjeldsen, P., Shao, L.-M., & He, P.-J. (2015). Quantification of regional leachate variance from municipal solid waste landfills in china. *Waste management*, *46*, 362–372.

Zhang, H., Hendricks Franssen, H.-J., Han, X., Vrugt, J. A., & Vereecken, H. (2017). State and parameter estimation of two land surface models using the ensemble kalman filter and the particle filter. *Hydrology and Earth System Sciences*, *21*(9), 4927–4958.

Zhang, J., Zhang, J.-m., Xing, B., Liu, G.-d., & Liang, Y. (2021). Study on the effect of municipal solid landfills on groundwater by combining the models of variable leakage rate, leachate concentration, and contaminant solute transport. *Journal of Environmental Management*, *292*, 112815.

Zhang, S., Liu, Z., Zhang, X., Wu, X., Han, G., Zhao, Y., ... others (2020). Coupled data assimilation and parameter estimation in coupled ocean–atmosphere models: a review. *Climate Dynamics*, *54*, 5127–5144.

Figure 5.

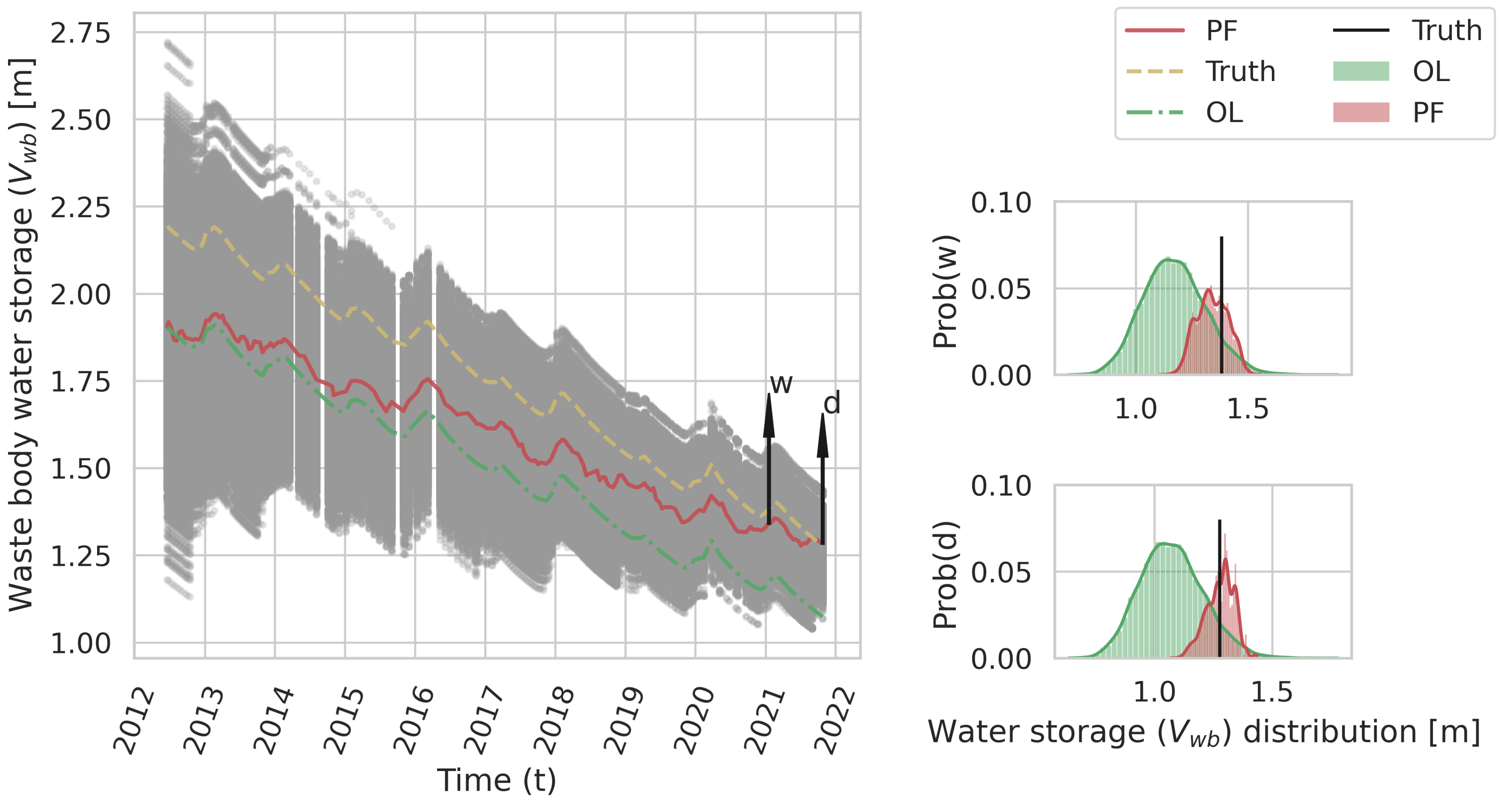

PF
Truth
OL
Truth
OL
PF
Waste body water storage (V_{wb}) [m]
2.75
2.50
2.25
2.00
1.75
1.50
1.25
1.00
2012
2013
2014
2015
2016
2017
2018
2019
2020
2021
2022
Time (t)
w
d
Prob(w)
Prob(d)
0.10
0.05
0.00
1.0
1.5
Water storage (V_{wb}) distribution [m]

Figure 3.

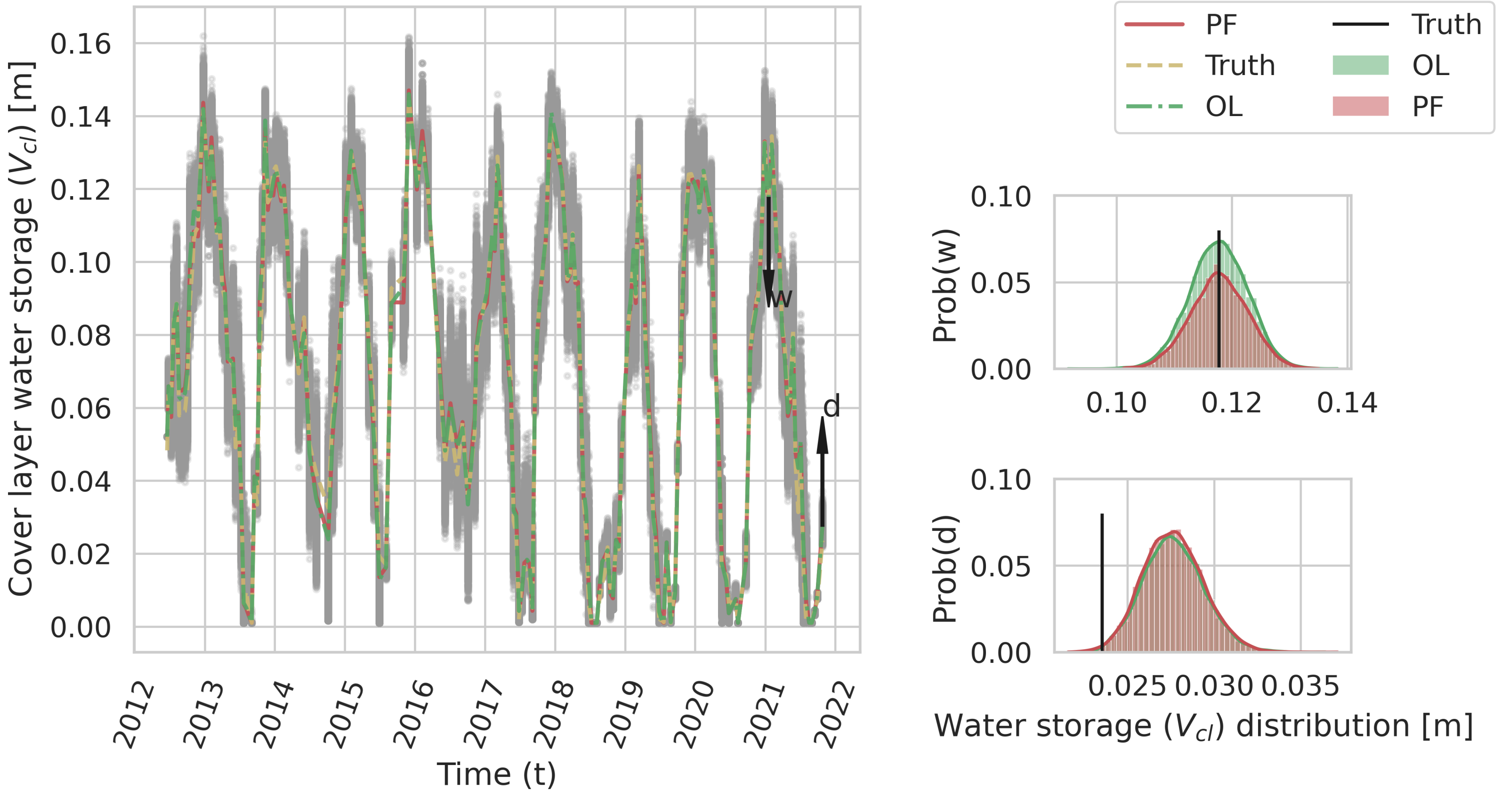

Cover layer water storage (V_{cl}) [m]
0.16
0.14
0.12
0.10
0.08
0.06
0.04
0.02
0.00
2012
2013
2014
2015
2016
2017
2018
2019
2020
2021
2022
Time (t)
w
d
PF
Truth
OL
Truth
OL
PF
Prob(w)
0.10
0.05
0.00
0.10
0.12
0.14
Prob(d)
0.10
0.05
0.00
0.025
0.030
0.035
Water storage (V_{cl}) distribution [m]

Figure 13.

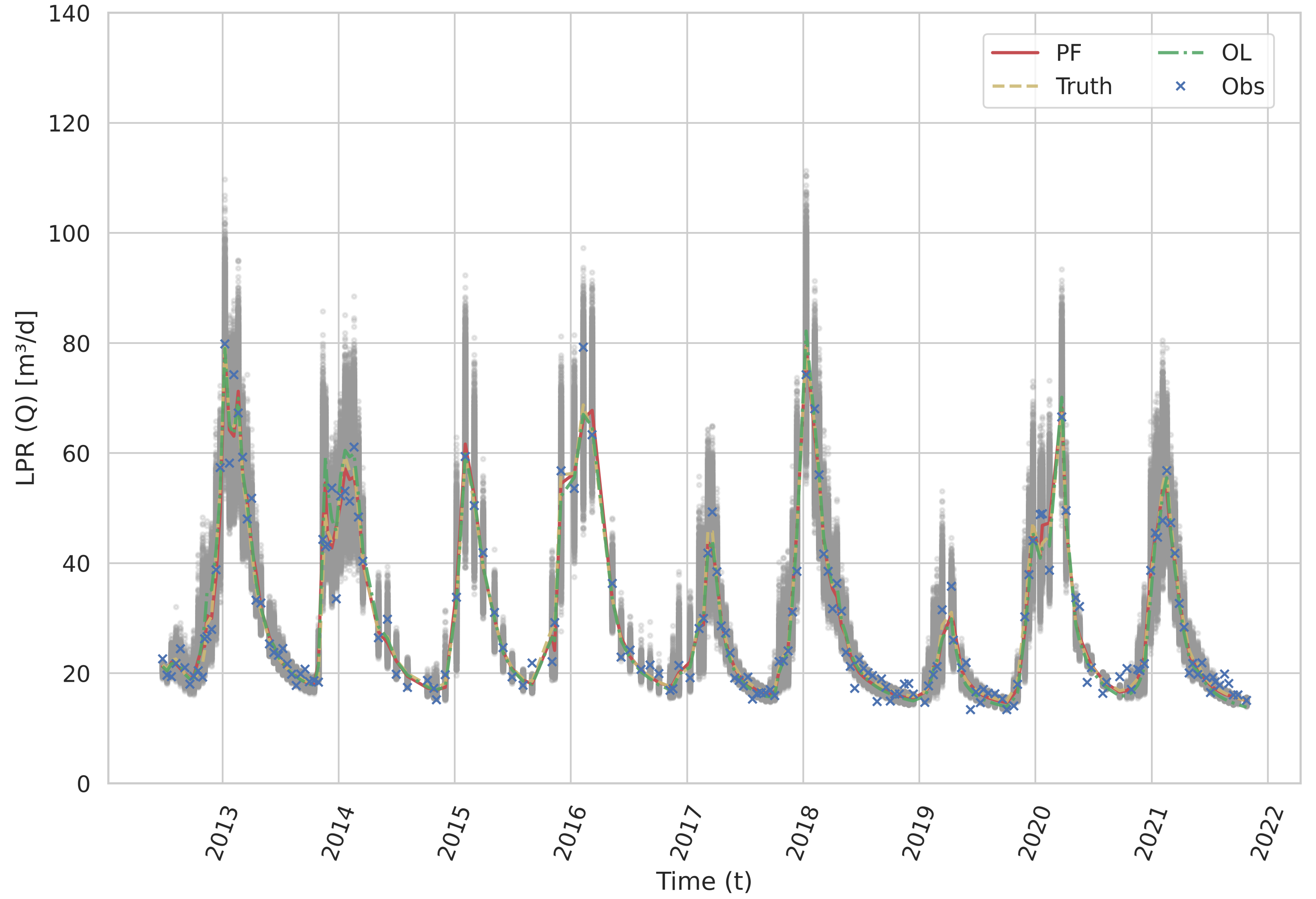

PF
OL
Truth
Obs
LPR (Q) [m³/d]
Time (t)
0
20
40
60
80
100
120
140
2013
2014
2015
2016
2017
2018
2019
2020
2021
2022

Figure 11.

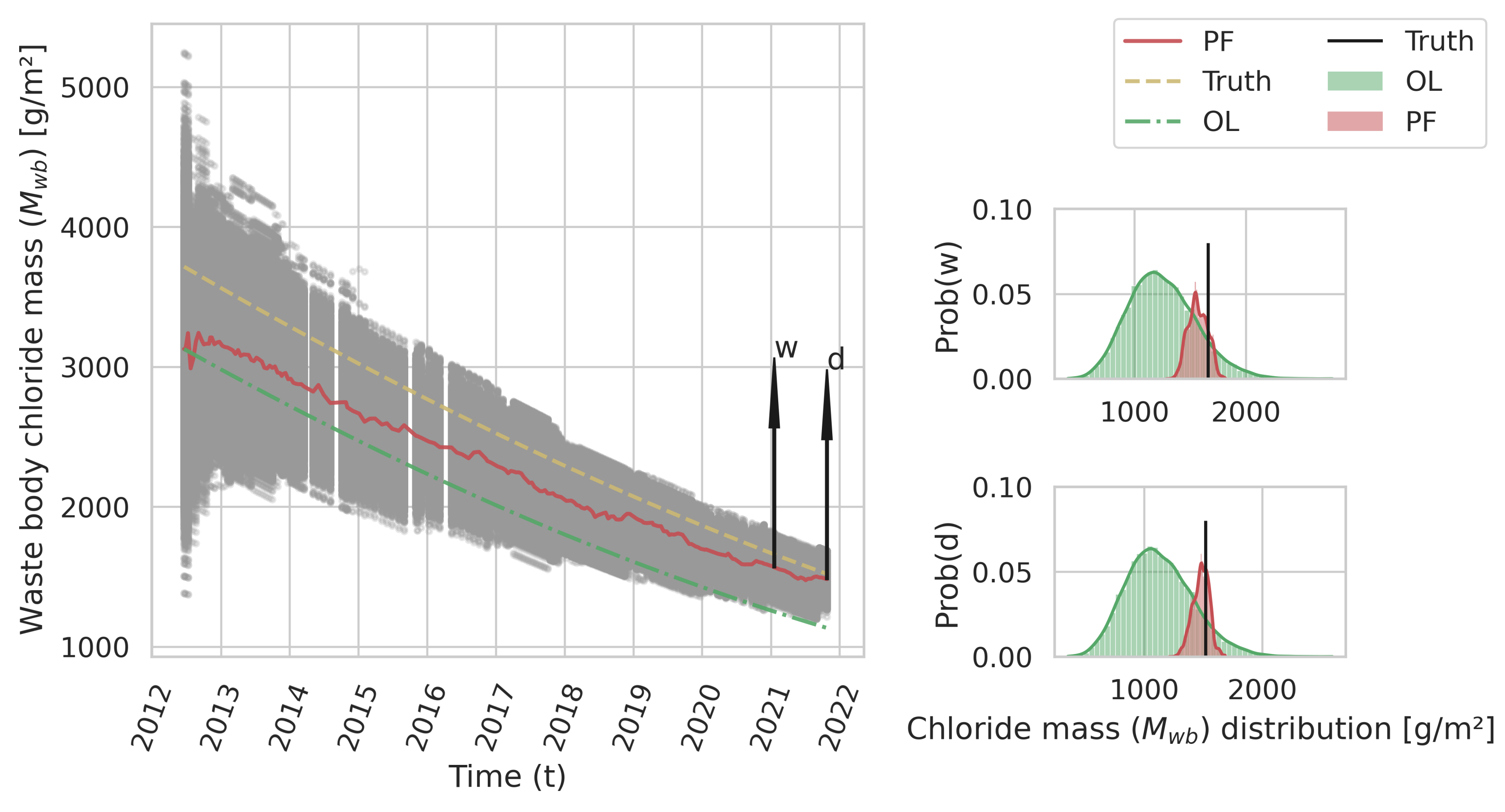

Waste body chloride mass (M_{wb}) [g/m²]
5000
4000
3000
2000
1000
w
d
2012
2013
2014
2015
2016
2017
2018
2019
2020
2021
2022
Time (t)
PF
Truth
OL
Truth
OL
PF
Prob(w)
0.10
0.05
0.00
1000
2000
Prob(d)
0.10
0.05
0.00
1000
2000
Chloride mass (M_{wb}) distribution [g/m²]

Figure 15.

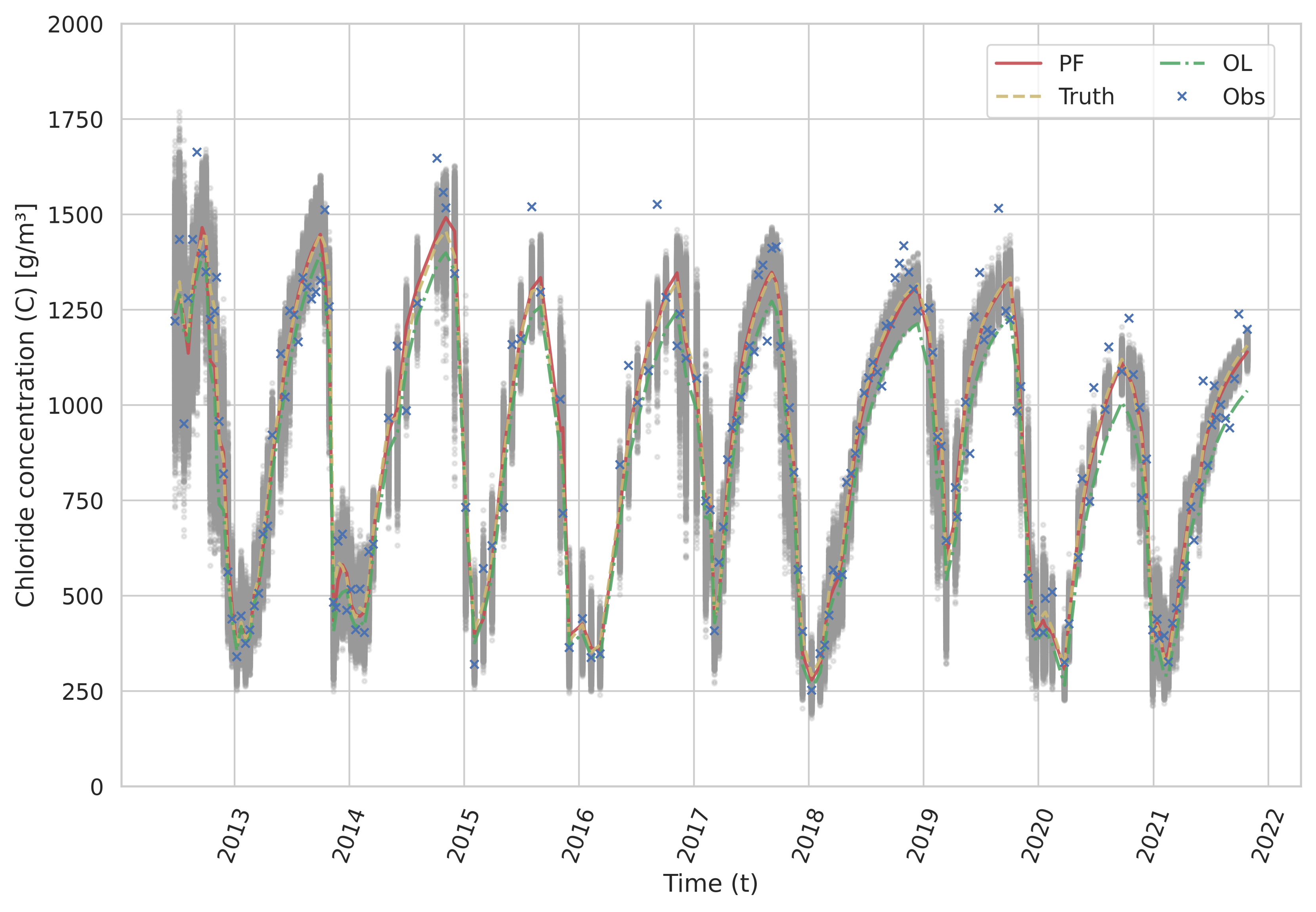
PF
OL
Truth
Obs
Chloride concentration (C) [g/m³]
Time (t)
2000
1750
1500
1250
1000
750
500
250
0
2013
2014
2015
2016
2017
2018
2019
2020
2021
2022

Figure 9.

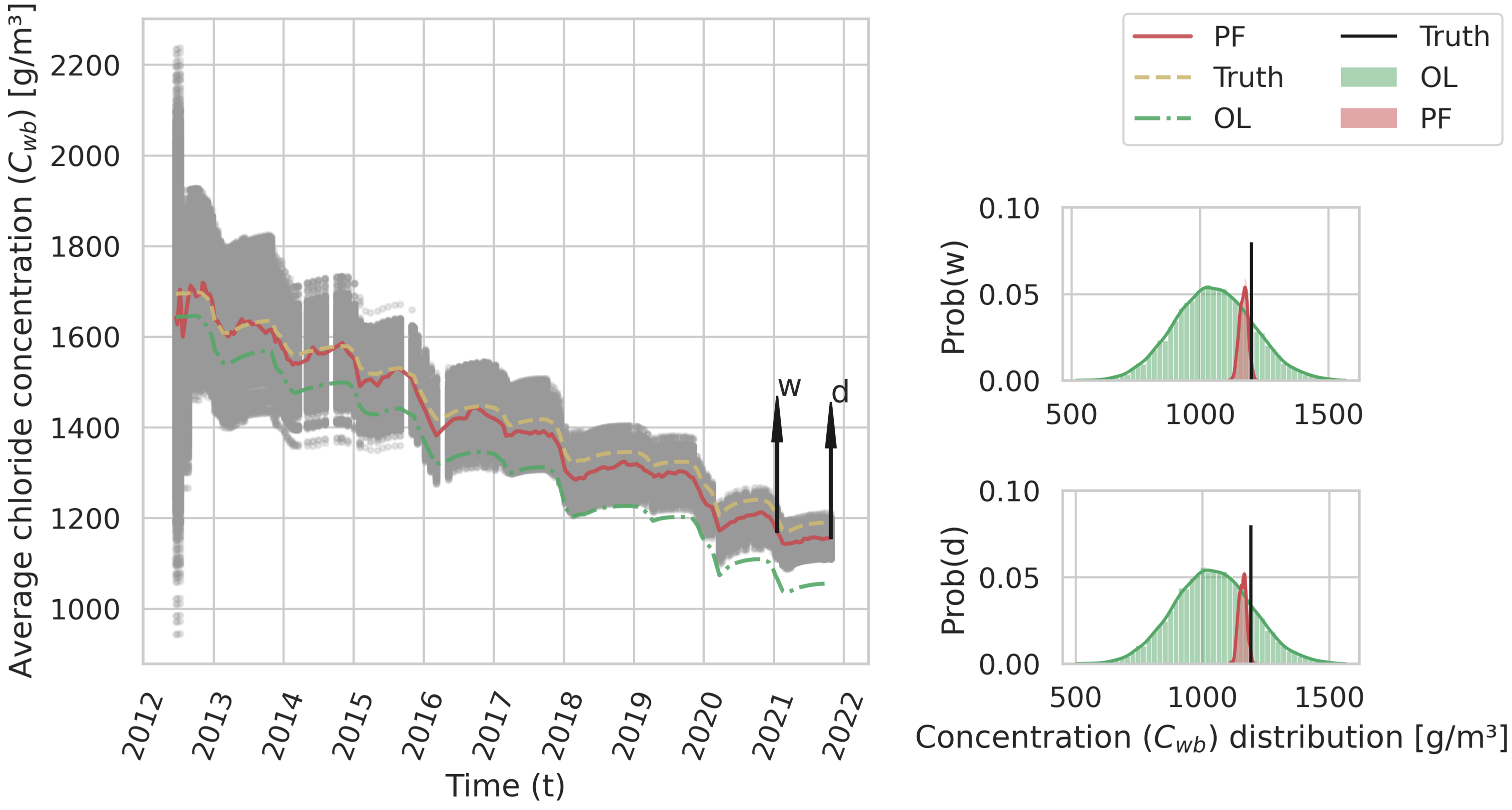

PF
Truth
OL
Truth
OL
PF
Average chloride concentration (C_{wb}) [g/m³]
Time (t)
w
d
Prob(w)
Prob(d)
Concentration (C_{wb}) distribution [g/m³]

Figure 4.

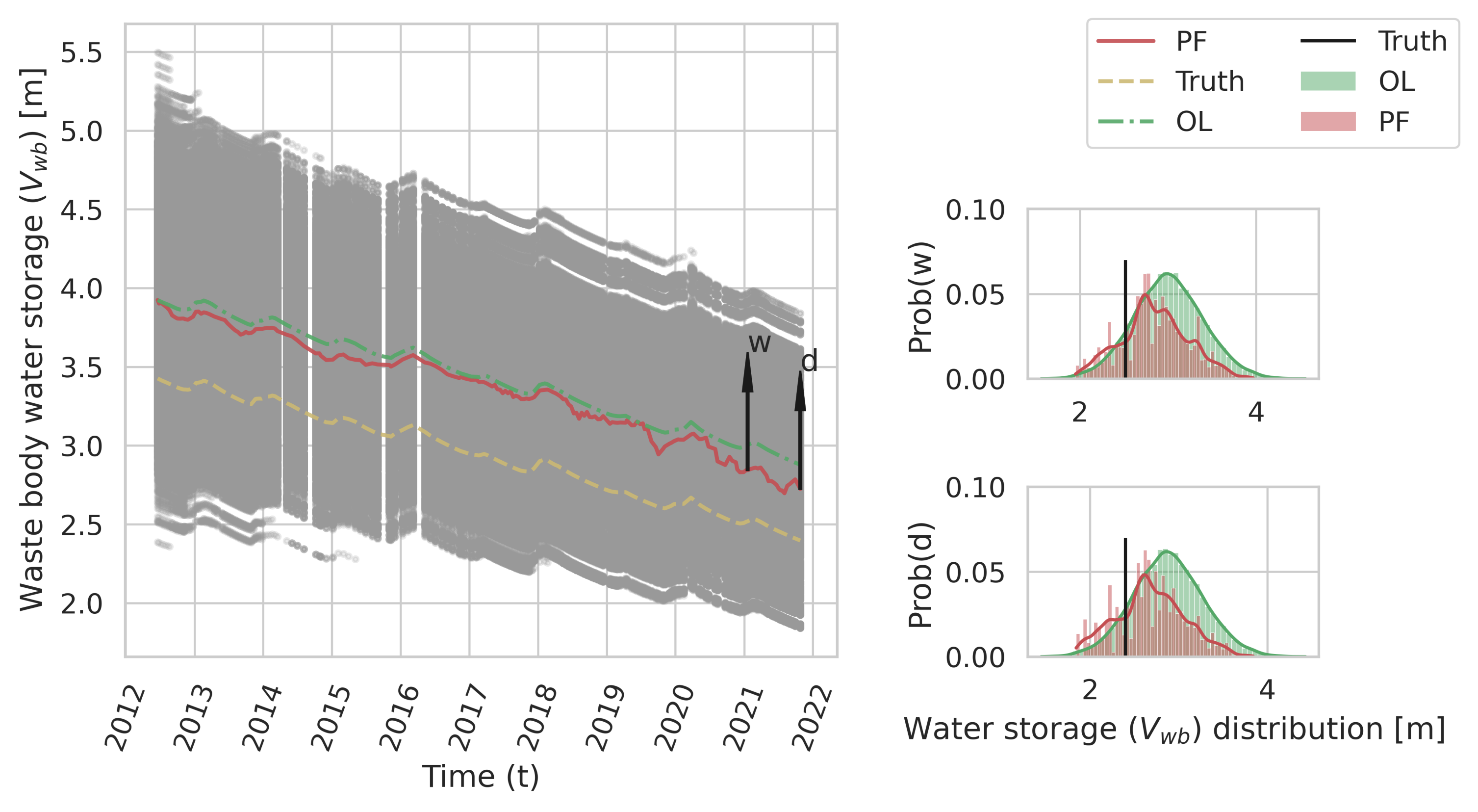

Waste body water storage (V_{wb}) [m]
Time (t)
w
d
PF
Truth
OL
Truth
OL
PF
Prob(w)
Prob(d)
Water storage (V_{wb}) distribution [m]

Figure 2.

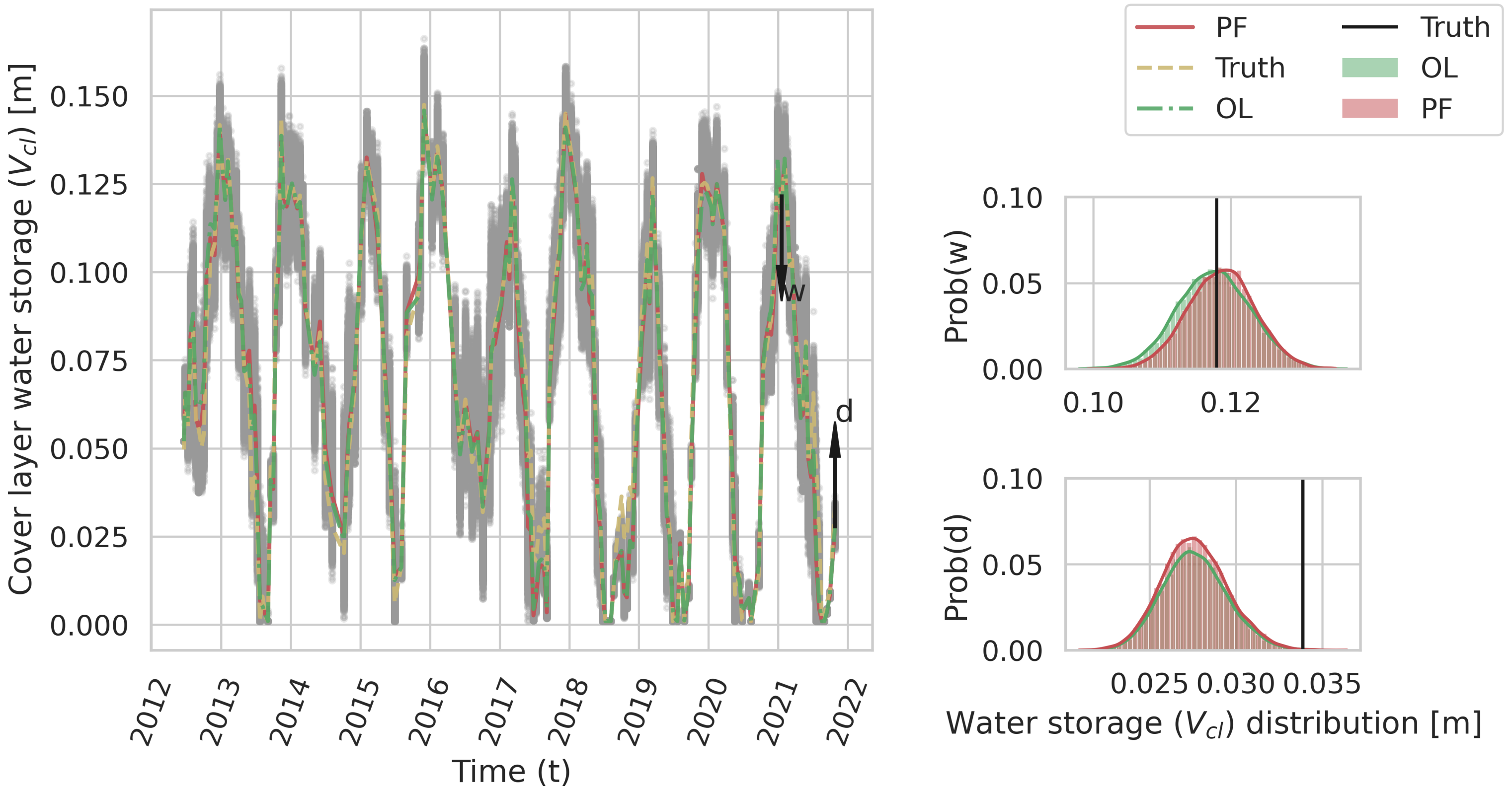

PF
Truth
OL
Truth
OL
PF
Cover layer water storage (V_{cl}) [m]
0.000
0.025
0.050
0.075
0.100
0.125
0.150
w
d
2012
2013
2014
2015
2016
2017
2018
2019
2020
2021
2022
Time (t)
Prob(w)
0.00
0.05
0.10
0.10
0.12
Prob(d)
0.00
0.05
0.10
0.025
0.030
0.035
Water storage (V_{cl}) distribution [m]

Figure 12.

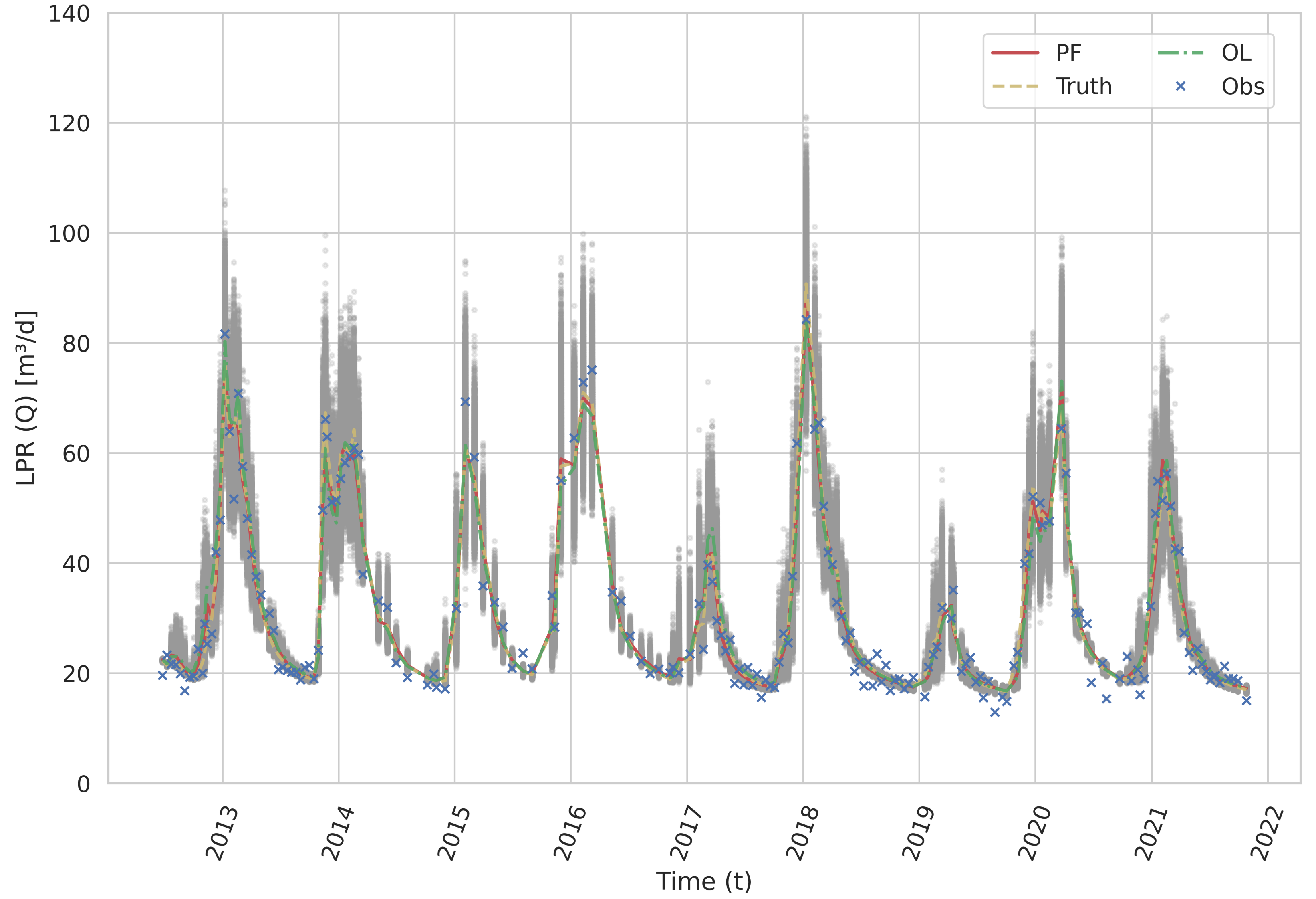
PF
OL
Truth
Obs
140
120
100
80
60
40
20
0
LPR (Q) [m³/d]
2013
2014
2015
2016
2017
2018
2019
2020
2021
2022
Time (t)

Figure 10.

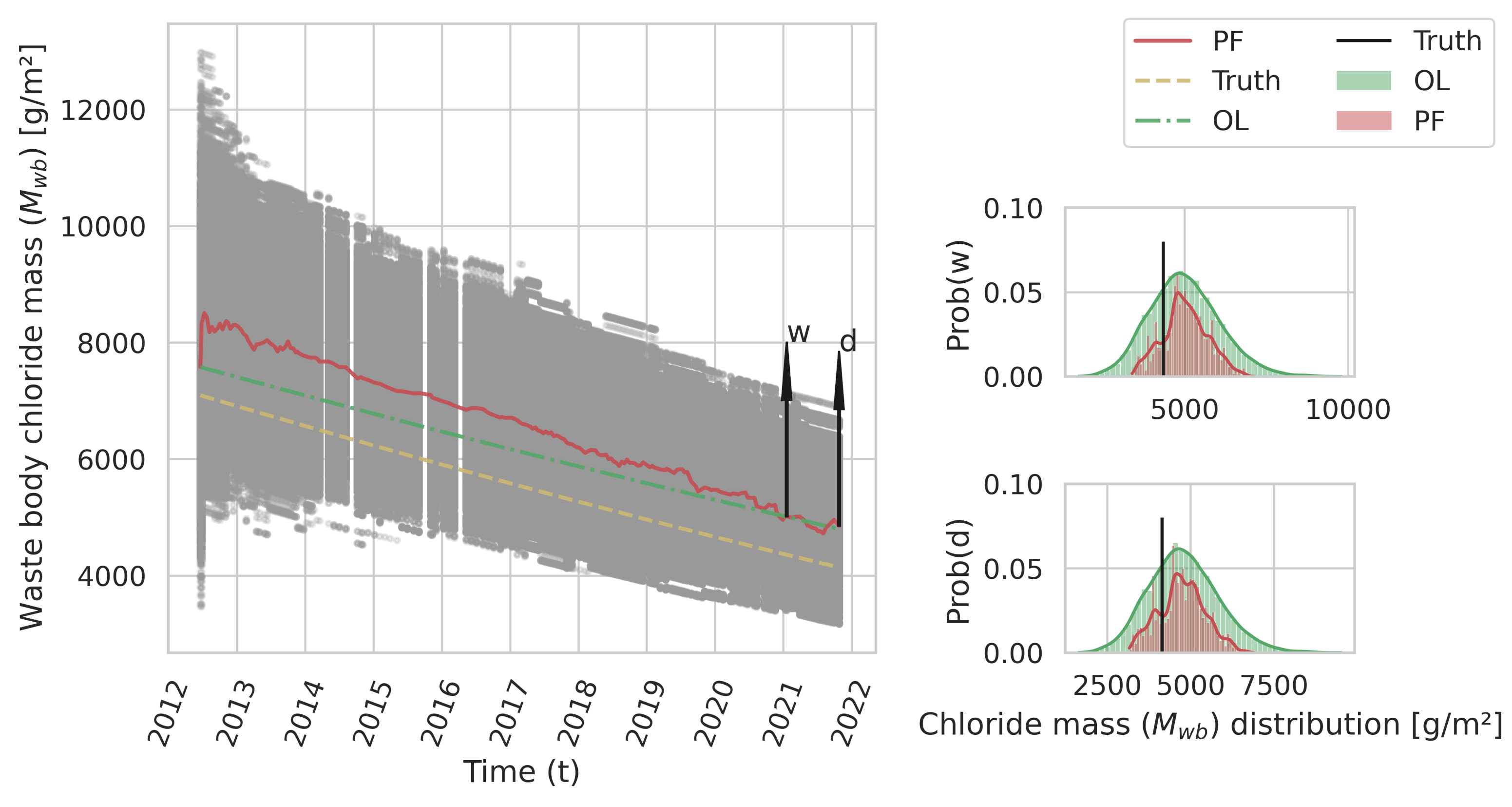

PF
Truth
OL
Truth
OL
PF
Waste body chloride mass (M_{wb}) [g/m²]
12000
10000
8000
6000
4000
w
d
2012
2013
2014
2015
2016
2017
2018
2019
2020
2021
2022
Time (t)
Prob(w)
0.10
0.05
0.00
5000
10000
Prob(d)
0.10
0.05
0.00
2500
5000
7500
Chloride mass (M_{wb}) distribution [g/m²]

Figure 14.

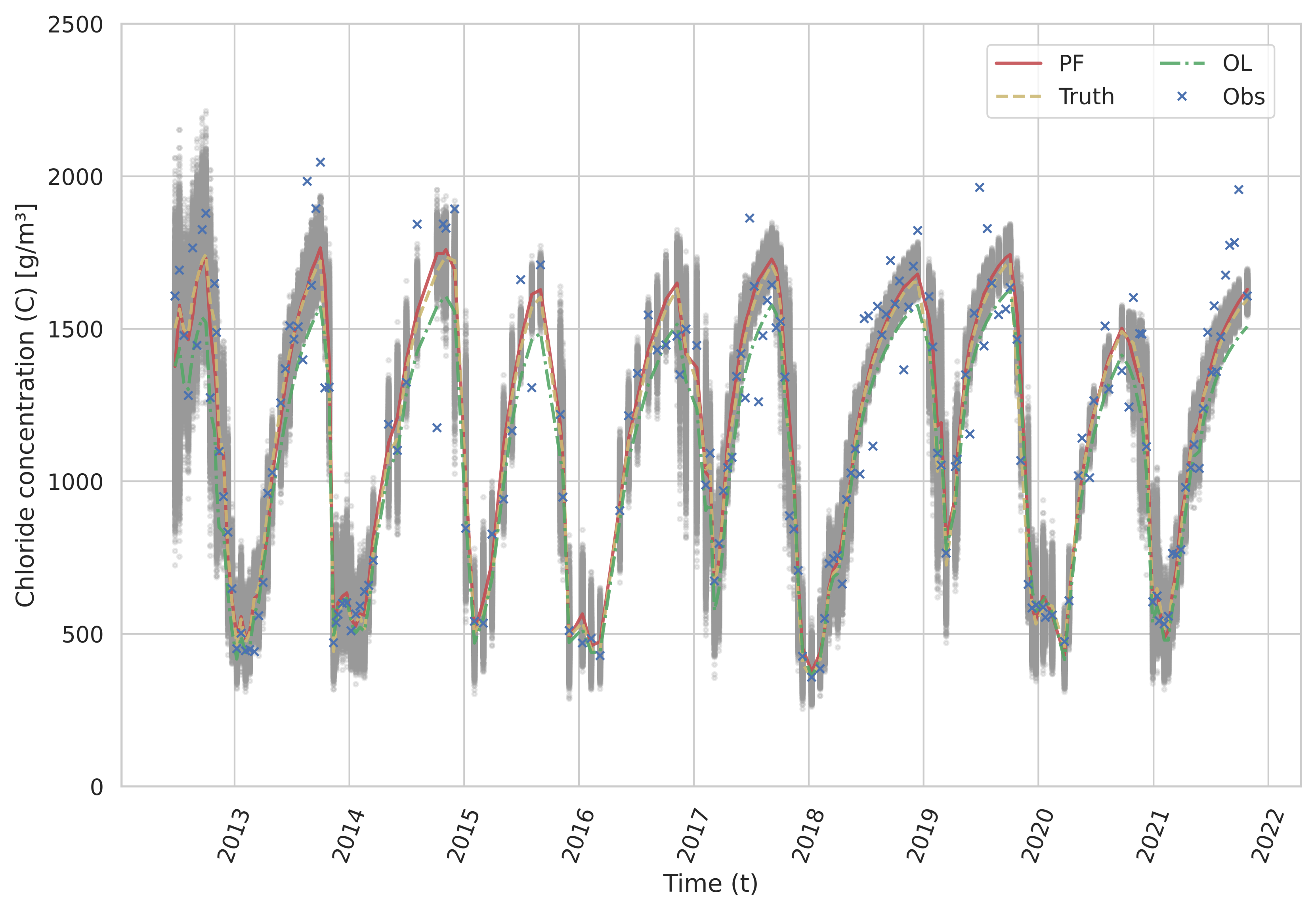
PF
Truth
OL
Obs
Chloride concentration (C) [g/m³]
Time (t)
0
500
1000
1500
2000
2500
2013
2014
2015
2016
2017
2018
2019
2020
2021
2022

Figure 8.

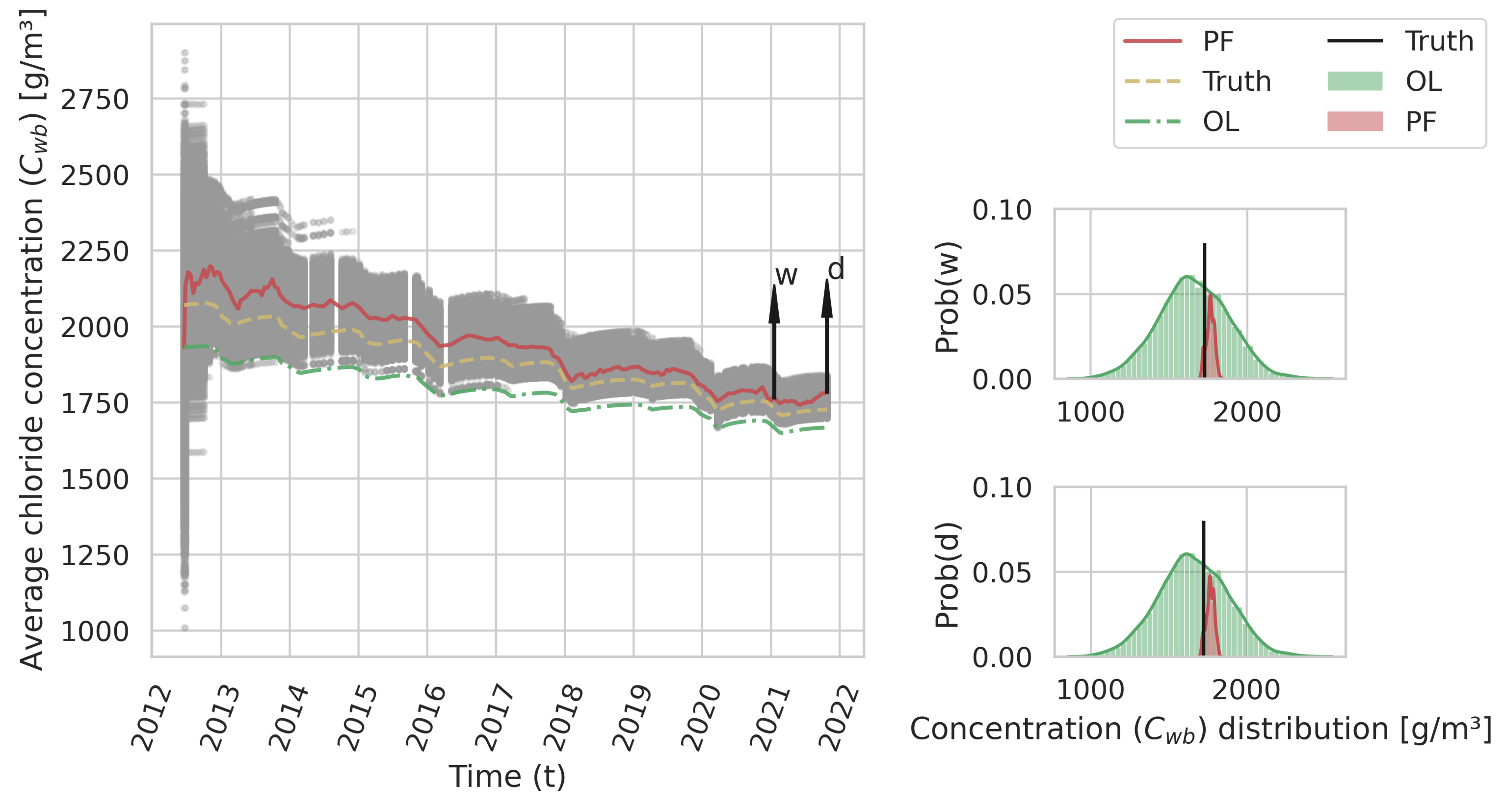

Average chloride concentration (C_{wb}) [g/m³]
2750
2500
2250
2000
1750
1500
1250
1000
2012
2013
2014
2015
2016
2017
2018
2019
2020
2021
2022
Time (t)
w
d
PF
Truth
OL
Truth
OL
PF
Prob(w)
Prob(d)
0.10
0.05
0.00
1000
2000
Concentration (C_{wb}) distribution [g/m³]

Figure 1.

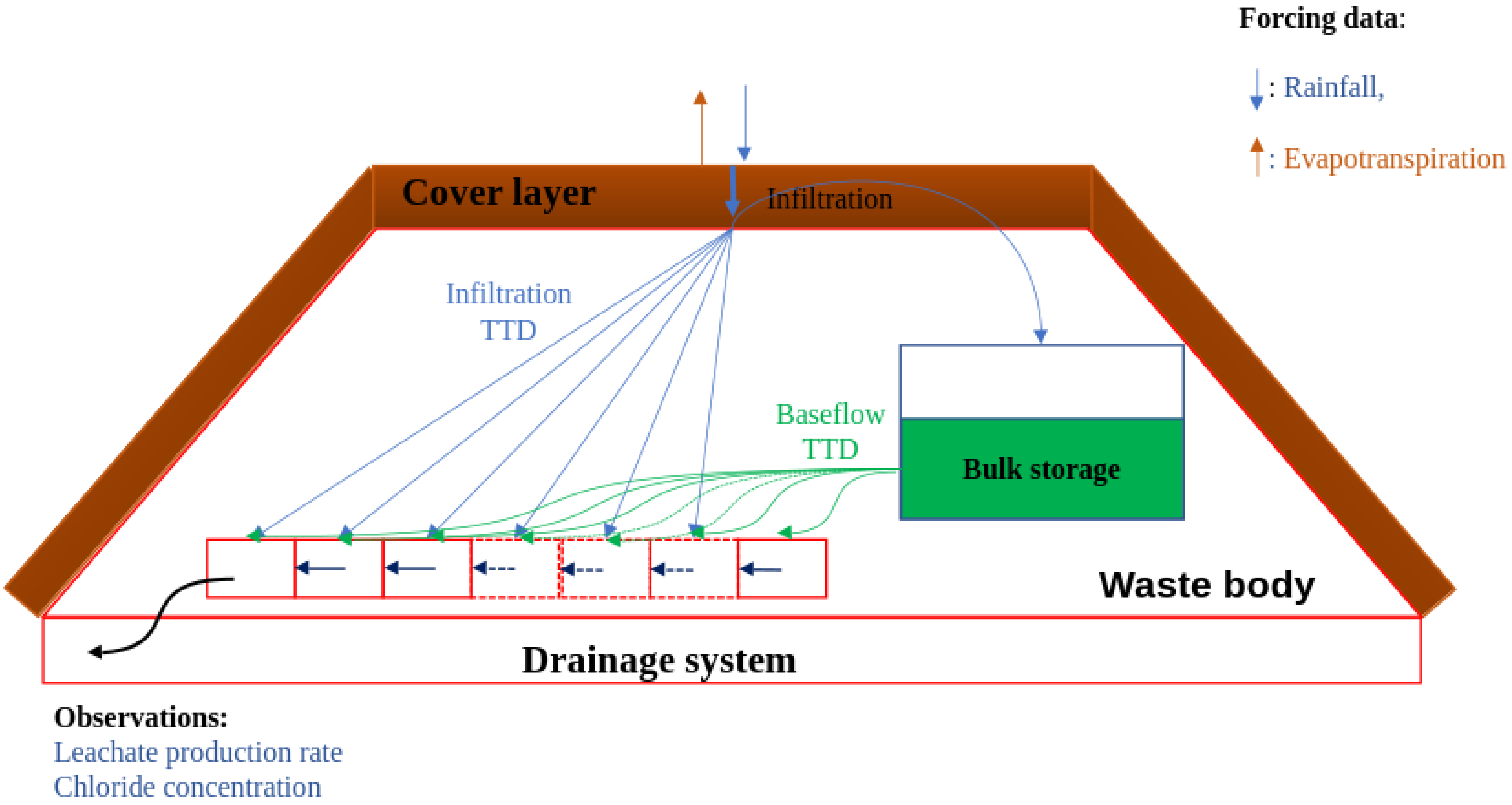
Forcing data:
: Rainfall,
: Evapotranspiration
Cover layer
Infiltration
Infiltration
TTD
Baseflow
TTD
Bulk storage
Waste body
Drainage system
Observations:
Leachate production rate
Chloride concentration

Figure 7.

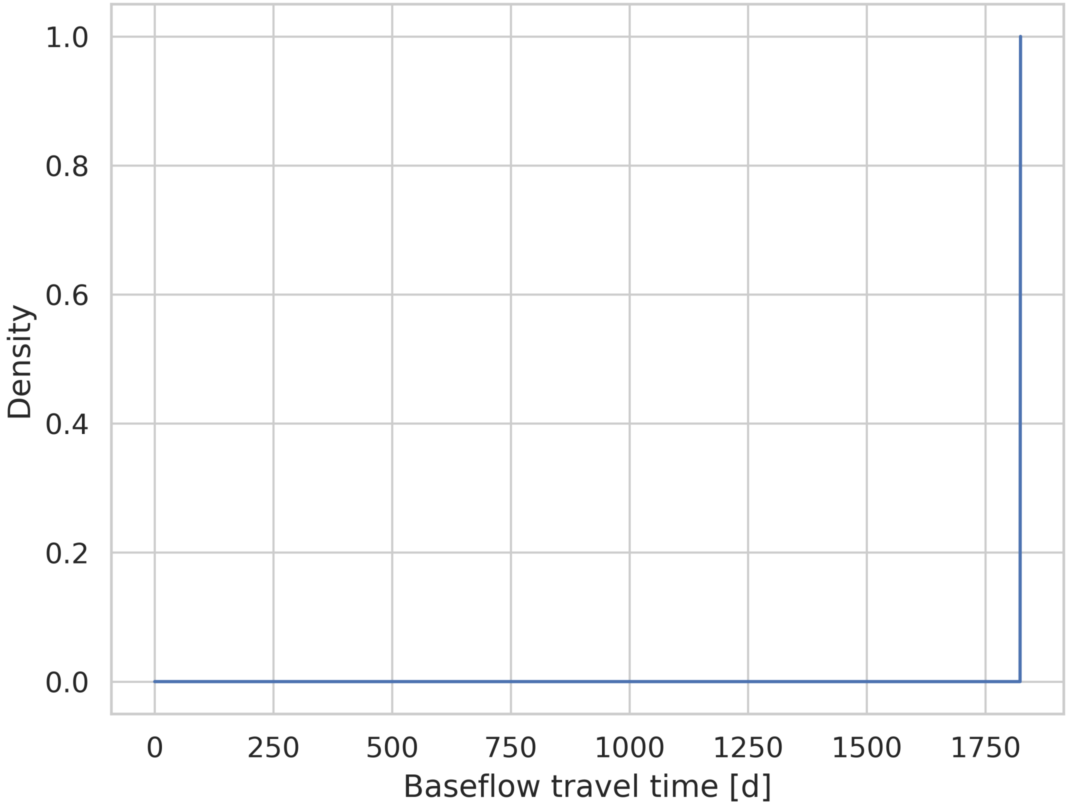
1.0
0.8
0.6
0.4
0.2
0.0
Density
0
250
500
750
1000
1250
1500
1750
Baseflow travel time [d]

Figure 6.

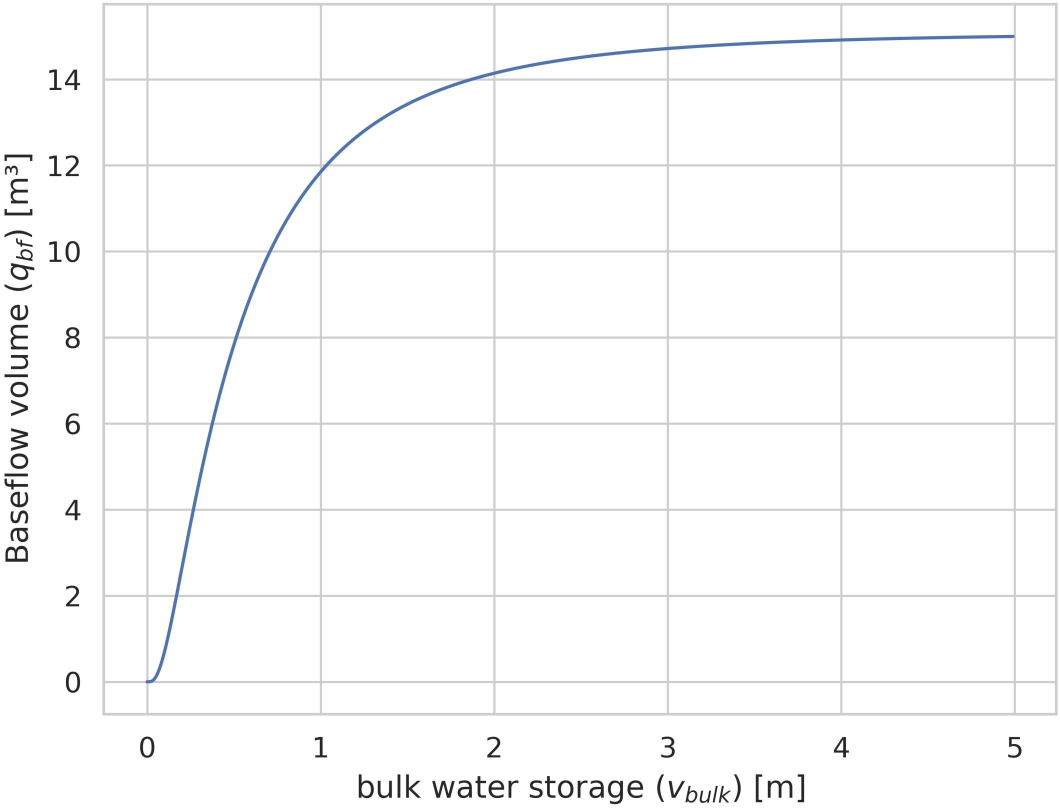

Baseflow volume (q_{bf}) [m³]
14
12
10
8
6
4
2
0
0
1
2
3
4
5
bulk water storage (v_{bulk}) [m]